


Science Paper

## Organic-rich Shales Reveal Local Controls That Enhanced Mercury Accumulation During a non-LIP Interval of the Miocene: Implications for the Mercury Paleoproxy

Theodore R. Them II<sup>1</sup><sup>a</sup>, Clara L. Meier<sup>1,2</sup>, Christopher J. Tino<sup>3,4</sup>, Marisa D. Knight<sup>1</sup>, Leanne G. Hancock<sup>3,5</sup>, Richard J. Behl<sup>6</sup>, Timothy W. Lyons<sup>3</sup>

<sup>1</sup> Department of Geology and Environmental Geosciences, College of Charleston, <sup>2</sup> HNTB Corporation, <sup>3</sup> Department of Earth and Planetary Sciences, University of California, Riverside, <sup>4</sup> Department of Earth, Energy, and Environment, University of Calgary, <sup>5</sup> Michigan Department of Environment, Great Lakes, and Energy, <sup>6</sup> Department of Geological Sciences, California State University, Long Beach

Keywords: Hg anomalies, redox, extinctions, massive volcanism, large igneous provinces

<https://doi.org/10.2475/001c.122687>

American Journal of Science

Vol. 324, 2024

Sedimentary mercury (Hg) concentrations are traditionally used to track atmospheric Hg deposition, which is thought to be controlled by volcanic outgassing and potentially the emplacement of large igneous provinces (LIPs). Sedimentary Hg enrichments are subsequently inferred to represent ancient intervals of massive volcanism and are often used to link the destabilization of Earth's environment to extinction. The biogeochemical cycling and controls on Hg sequestration in sediments, however, are both dynamic and complex, with wide spatiotemporal variability. To better elucidate the controls on Hg cycling, sediments from the Miocene Monterey Formation were studied in three separate sedimentary basins (San Joaquin Basin [SJB], Santa Barbara Basin [SBB], Santa Maria Basin [SMB]) from the eastern Pacific margin, representing approximately seven million years of quasi-contemporaneous deposition under predominantly reducing conditions during a non-LIP interval. Furthermore, the sites were located in close proximity to terrestrial volcanic centers. The modes of Hg delivery and sequestration were generally different in each of these basins. In the proximal SJB, Hg contents were related to aluminum and pyrite concentrations, which are proxies for aluminosilicate/detrital input and relative degrees of sulfate-reducing conditions in sediments and water column, respectively. In the more distal SMM and SBB, Hg contents were controlled by the amount of pyrite burial and organic matter concentrations, respectively. In the SBB, however, two clear populations of geochemical data suggest a shift in the contribution of Hg-enriched detrital materials to this basin controlling Hg delivery or variations in Hg scavenging efficiency. These multiproxy relationships make it clear that a range of geochemical proxies applied in multiple syndepositional settings with different environmental conditions should be used in tandem to distinguish local versus global controls on Hg deposition. We suggest that biogeochemical feedbacks during intervals of massive volcanism in the past, related to changes in weathering and erosion of soils on land and local redox, may be a critical if not dominant driver of sedimentary Hg enrichments. These observations highlight the importance of ruling out local to regional processes that can enrich sediments in Hg before ascribing massive volcanism as the foremost source of excess mercury in shale sequences.

### 1. INTRODUCTION

Mercury (Hg) is a redox-sensitive element (RSE) with a strong affinity for some clay minerals (e.g., Frieling et al., 2023; Kongchum et al., 2011; Ravichandran, 2004). Due to its behavior as an RSE, Hg can accumulate preferentially in sulfidic sediments and euxinic (anoxic and sulfidic) water columns during iron sulfide (e.g., pyrite) formation and burial (e.g., Bower et al., 2008; Duan et al., 2016; Frieling

et al., 2023; Ravichandran, 2004; Shen et al., 2020). Despite its strong affinity for sulfide and some clay minerals, sedimentary Hg enrichments have been used as a proxy to track the ancient emplacement of large igneous provinces (LIPs) or flood basalts (see review by Grasby et al., 2019). To date, sedimentary Hg enrichments observed across several Phanerozoic climatic perturbations and (mass) extinction events have been attributed to LIP emplacement, even in cases where there is no other geological evidence for wide-

<sup>a</sup> Corresponding author: themtr@charleston.edu

spread volcanism (see Y. Liu et al., 2023; Shen et al., 2019). The overriding assumption is that sedimentary Hg enrichments represent intervals of increased atmospheric loading of Hg by LIP outgassing.

Mercury also complexes readily with organic matter (OM) as confirmed by its strong affinity and enhanced stability constants in many modern environments (Lavoie et al., 2019; Ravichandran, 2004). Therefore, an increase in Hg concentrations may simply reflect an increase in sedimentary organic matter (generally measured as total organic carbon or TOC). This relationship necessitates the normalization of Hg to TOC (displayed as Hg/TOC) to eliminate the possibility that Hg enrichments are simply the product of variably high TOC contents (see Grasby et al., 2019; Percival et al., 2021). Under euxinic conditions, however, where pyrite formation and thus uptake of sulfide is often limited by the availability of reactive Fe, Hg can be enriched relative to TOC because of water column sulfide formation and accumulation and Hg uptake in a sulfide phase such as pyrite (and potentially other authigenic minerals). This process can be decoupled from local TOC delivery, similar to molybdenum (Mo) cycling (e.g., Berner, 1984; Lyons & Berner, 1992). This is potentially why C/S values can be low in euxinic settings yet still be associated with Hg/TOC enrichments. Sedimentary Hg and Hg/TOC enrichments are commonly discussed in terms of excesses relative to a global Phanerozoic average (see Grasby et al., 2019). It is more important, however, to consider them with respect to long-term baseline values for the specific basin. In this context, many intervals with reported Hg and Hg/TOC enrichments are not anomalous relative to their respective Phanerozoic average that define a global baseline and instead suggest enrichments may be controlled by local factors rather than greatly elevated, broad Hg inputs (e.g., Pruss et al., 2019; Them et al., 2019).

Ancient climatic and environmental perturbations are often associated with the deposition of sediments under anoxic/reducing conditions in many regions of the oceans with variable TOC concentrations (e.g., Jenkyns, 1988; Ostrander et al., 2017; Owens et al., 2018; Them et al., 2017, 2019). In oxygenated environments, RSE accumulation is linked to Fe-Mn oxide deposits. With a transition to reducing conditions, the biogeochemical cycling of RSEs such as Hg is shifted, with its sequestration likely controlled by sulfide minerals or organic matter (e.g., Y. Liu et al., 2023; Shen et al., 2019; Them et al., 2019). Based on these known transitions in depositional environments, it is possible that Hg accumulation in sediments was controlled by redox and pyrite burial more so in the past than today, which instead is marked by observations of Hg that is predominantly associated with organic matter. Changes in local redox conditions are commonly manifested as a change in mineralogy and lithology (e.g., organic matter-lean limestones to OM-rich, pyritic siliciclastic shales), although petrographic, mineralogical, and geochemical data should be used to confirm this transition. Furthermore, changes in grain size may also impact the biogeochemical cycling of Hg (e.g., Das et al., 2013; Moore et al., 2019), likely due to different min-

eral assemblages that can impact porosity and permeability, which affect pore water chemistry.

Until recently, there were few studies that measured pyrite concentrations of ancient sediments that contained Hg anomalies, which may have led to inaccurate estimates of the role of pyrite in Hg enrichment. Studies that have paired direct pyrite data with Hg anomalies have shown a strong relationship between the two, pointing to local processes that may also increase Hg loading in sediments—for example, during the Toarcian Oceanic Anoxic Event (Early Jurassic, e.g., Them et al., 2019) and Late Ordovician mass extinction (e.g., Shen et al., 2019). In addition, global sedimentary Hg compilations viewed in the context of basin transects have also revealed distinct trends between Hg/TOC magnitude and relative distance from a landmass (e.g., Them et al., 2019; Tremblin et al., 2022). In this light, it seems best, before assuming a volcanogenic driver for Hg enrichment, to reconstruct past Hg cycling in detail by compiling multiproxy datasets (including redox and detrital inputs) that allow us to consider other processes that can generate sedimentary Hg enrichments and associated Hg/TOC anomalies (e.g., C. N. Bowman et al., 2021; Grasby et al., 2019; Hagen et al., 2022; Percival et al., 2018; Pruss et al., 2019; Shen et al., 2019, 2020; Them et al., 2019).

The association of anoxic/reducing conditions and preponderance of organic matter-rich shales with ancient intervals of global environmental change necessitate studies that focus on the behavior of Hg in similar environments of different ages across non-LIP intervals (see Percival et al., 2018, for discussion of Hg cycling across LIP intervals). LIP intervals are fundamentally different than those described here because of the large magnitude of LIP volcanism is suggested to directly increase the atmospheric flux of Hg to Earth's surface, culminating in large sedimentary Hg/TOC enrichments (see Grasby et al., 2019). This comparison will ultimately lead to more accurate interpretations of ancient Hg geochemical records (e.g., Grasby et al., 2019; Percival et al., 2018; Shen et al., 2020). There are no modern environments that have remained predominantly anoxic and reducing for timescales generally associated with ancient intervals of global environmental destabilization ( $10^4$ – $10^6$  yr), so this study focuses on marine sedimentary deposits from the eastern Pacific Ocean that accumulated during the Miocene in predominantly anoxic basins.

In this contribution, we measured Hg concentrations in over 400 samples of the Miocene Monterey Formation (MMF) in California from three sections (outcrop and drill core) of OM-rich shales deposited under predominantly reducing conditions. These sites were chosen because they represent multi-million-year intervals of quasi-homogeneous redox conditions (anoxic and sometimes euxinic) and deposition of fine-grained sediments in marginal marine environments (e.g., Hancock et al., 2019) that accumulated after the eruption of the Columbia River flood basalts. The destruction of ocean crust through subduction necessitates studies that focus on these more marginal/proximal environments (i.e., in close proximity to landmasses), as the deeper in time we go, the number of open ocean sedimen-

tary sections encountered decreases because of subduction and a related tectonic bias toward preservation of continental margin settings. The majority of sections that are available to study that are Mesozoic or older in age tend to be located in marginal, epeiric, or epicontinental environments. Therefore, the marginal environments in this study are similar to the majority of those targeted for more ancient events that are used to reconstruct the Hg cycle. We have paired these data with published redox and detrital proxy datasets (Hancock et al., 2019) and some additional results generated in this study to identify the mechanism(s) that controlled Hg sequestration in three basins in the middle to late Miocene (see Shen et al., 2020). The results and trends reveal a unique perspective on the complex and dynamic biogeochemical cycling and sequestration of Hg in sediments that is largely not reflected in the existing literature. Although these study locations are geographically adjacent, Hg accumulation in each basin was linked to different mechanisms. Last, our multi-proxy datasets provide evidence that many of the standard and indirect methods employed to reconstruct local changes in pyrite formation and burial can be unreliable. In cases where total iron, total sulfur, or molybdenum concentrations are used to estimate the influence of local redox variations on Hg accumulation, these proxies may under- or overestimate the role that pyrite formation and burial has on Hg sequestration in sediments.

## 2. THE MIOCENE

The Miocene Epoch is a critical interval during the greater Cenozoic Era when significant variation in global and regional climate occurred, possibly driven by a combination of changes in ocean circulation, ice sheet extent, and carbon cycling (Flower & Kennett, 1994; Herold et al., 2012; Holbourn et al., 2015; von der Heydt & Dijkstra, 2008; Zachos et al., 2001; many others). The transition from the early to middle Miocene is associated with elevated atmospheric  $p\text{CO}_2$  levels and warmer atmospheric and oceanic temperatures referred to as the Miocene Climatic Optimum (MCO; e.g., Holbourn et al., 2015). It has been hypothesized that the MCO was driven by volcanic outgassing of  $\text{CO}_2$  associated with the deposition of the Columbia River Basalt Group (e.g., Barry et al., 2013; Kasbohm & Schoene, 2018; Sosdian et al., 2020; Steinthorsdottir et al., 2021). Following the MCO, atmospheric  $p\text{CO}_2$  levels decreased, and the planet cooled from the middle to late Miocene in a series of steps, with long-term cooling interrupted by transient (*ca.* <100-kyr) warming-cooling episodes (e.g., Holbourn et al., 2013; Pagani et al., 1999; Westerhold et al., 2005; Wright et al., 1992; Zachos et al., 2001; many others). The general instability of the Miocene climate is likely the result of the interplay between multiple biogeochemical feedbacks and forcings within the Earth system (e.g., ocean gateways, carbon cycling, planetary albedo, biological innovations, etc.), all of which have the capacity to affect the others on both short and long timescales. Given this complexity, traditional and emerging proxies used in combination may allow us to track some or all of these possible drivers and feed-

backs, resulting in a more accurate and nuanced picture of the forcing factors behind global environmental change.

## 3. MERCURY CYCLE

On short timescales, the main source of Hg to the atmosphere is from the ocean (see [fig. 1](#) for flux estimations). The ocean, however, receives its largest flux of Hg from rivers (e.g., M. Liu et al., 2021) and wet and dry deposition from the atmosphere (e.g., Holmes et al., 2010). Riverine-derived Hg is sourced from biomass, biomass burning, soil and rock erosion/weathering, and the atmosphere (e.g., Amos et al., 2014; Schuster et al., 2018). Another potential source of Hg to the oceans is from hydrothermal fluids (e.g., K. L. Bowman et al., 2015; Kim et al., 2022), although their contributions to the atmospheric reservoir are not known. On long (geologic) timescales, the sources of Hg to oceans and atmosphere are assumed to be from subaerial and subaqueous volcanoes, the oxidative weathering of soils and rocks and transport via rivers, biological cycling, and delivery through cosmic dust and bolides (see Driscoll et al., 2013).

Due to the short residence time of Hg in the atmosphere (< 1 year, e.g., Driscoll et al., 2013; Selin, 2009), sedimentary Hg enrichments have traditionally been used as an indicator of past volcanic activity (see review by Grasby et al., 2019). In-depth reviews of the modern and ancient Hg cycle reveal a complex system that involves multiple transportation pathways and transient sinks before ultimate deposition in sedimentary rocks, which makes it difficult to determine the source of Hg in both modern and ancient sediments ([fig. 1](#); see Batrakova et al., 2014; Bessinger, 2014; Blum et al., 2014; Driscoll et al., 2013; Fitzgerald & Lamborg, 2014; Grasby et al., 2019; Percival et al., 2018; Selin, 2009; Sun et al., 2019; Them et al., 2019; Zhu et al., 2018). For example, Hg can be stored in organic matter (both micro- and macro-scale life; deceased or living), soils/floodplains, and snow/ice, with the potential to be cycled within or between any of these reservoirs multiple times before sequestration in a geologically stable sink such as sediments (see [fig. 1](#); e.g., Driscoll et al., 2013; Fitzgerald & Lamborg, 2014). For ancient intervals, the addition of complementary geochemical data can be integrated with Hg concentrations to determine the host phase or final pathway in the Hg cycle before ultimate deposition in sediments (e.g., Grasby et al., 2019; Shen et al., 2019, 2020; Them et al., 2019).

## 4. BACKGROUND

### 4.1. Monterey Formation geologic framework

The Miocene Monterey Formation (MMF) has been the focus of many sedimentological, geochemical, and stratigraphic studies since the mid-20th century (e.g., Behl, 1999; Bramlette, 1946; Föllmi et al., 2005, 2017; Garrison & Graham, 1984; Graham & Williams, 1985; Hancock et al., 2019; Isaacs et al., 1983; Lau et al., 2022; Woodring & Bramlette, 1950). MMF deposits accumulated in the eastern Pacific Ocean along the western continental margin

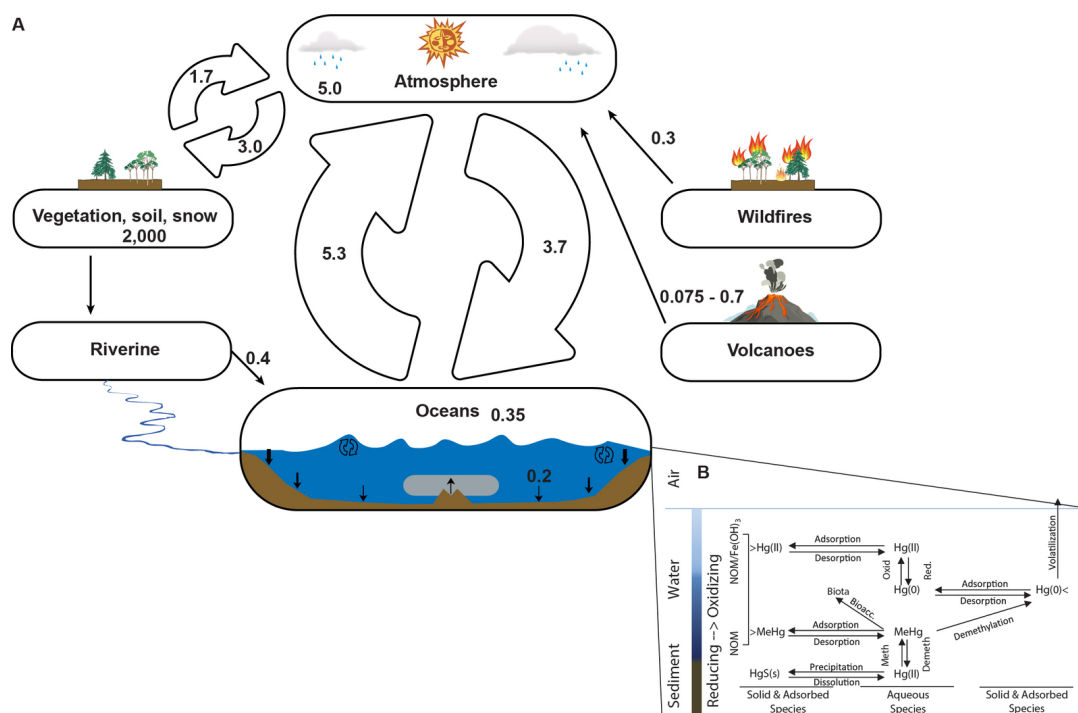


**Figure 1. Mercury cycle. A) Global mercury cycle (figure modified from Them et al., 2019). Values in mass balance (Hg reservoirs are Gg Hg yr<sup>-1</sup> and fluxes are Gg Hg yr<sup>-1</sup>) from Schuster et al. (2018) and references therein. B) Local mercury cycle (figure modified from Bessinger, 2014). Mercury can be transformed in aqueous environments under different redox regimes (see Tisserand et al., 2022).**

of North America (fig. 2). Deposition of the MMF and its equivalents spanned major changes in Miocene paleoceanography, climate, and tectonics (Barron, 1986; Ingle, 1981), and these changes are reflected in the large-scale lithostratigraphy of the Formation (Pisciotta & Garrison, 1981). Specifically, the predominantly diatomaceous and OM-rich Monterey sediments were deposited across a temporal transition in global marine thermohaline circulation patterns, which represents an important middle Miocene cooling step (Kennett, 1977; Zachos et al., 2001), toward a configuration that is more analogous to modern oceans. This modern configuration is marked by deep water that forms in the North Atlantic and circum-Antarctic regions and upwells principally in the Pacific and Indian Oceans (Flower & Kennett, 1994; Woodruff & Savin, 1989).

Although noted for its highly siliceous and OM-rich composition, MMF lithologies are heterogeneous and predominantly composed of interbedded calcareous, dolomitic, phosphatic or siliceous mudstone, diatomite, chert, porcellanite, and dolomite, with lesser and often localized presence of sandstone or volcanic ash (Behl, 1999; Föllmi et al., 2017). The MMF was deposited all along the western North American margin but accumulated in greatest thicknesses in distinct basins that ranged from isolated to fully connected to the open ocean (fig. 2). In these settings, deposition occurred under productive waters that yielded anoxic, reducing environments, contributing to enhanced organic matter (OM) preservation and high TOC contents (e.g., Föllmi et al., 2017; Hancock et al., 2019; Pytte, 1989). Organic matter is predominantly Type 1 to Type 2, consisting of marine algae, bacteria, and other

plankton (Pytte, 1989). The studied sections can be tied at least generally to regional and global biostratigraphic zones in the Miocene (Barron & Isaacs, 2001; Föllmi et al., 2017), but the biostratigraphy and chemostratigraphy in the sections have not shown any diagnostic fossils or features, respectively, that allow for higher-resolution correlations (see Föllmi et al., 2017; Hancock et al., 2019). This limited level of correlation nonetheless permits some portions of the studied sections to be placed in intervals of several million-years duration that overlap temporally with one another (e.g., Föllmi et al., 2017; Hancock et al., 2019). Within this general framework, we studied the San Joaquin Basin (SJB; Thorndyke core; one absolute age of 11.56 Ma, duration unknown), Santa Maria Basin (SMB; Union Leroy 51–80 core, ~13.5–10 Ma), and Santa Barbara Basin (SBB; Naples Beach section; ~14.26–9.46 Ma) (fig. 2) to determine the controls on Hg cycling at each site (see Hancock et al., 2019, for supporting details about the age model for each study site).

Two of the study sites were previously subdivided into chemostratigraphic intervals based on lithology and metal geochemistry (e.g., Hancock et al., 2019). Specifically, SJB is divided into SJB1, SJB2, and SJB3; SMB is divided into SMB1 and SMB2; SBB is divided into the lower section and upper section. These divisions were based on inferred transitions among different redox environments (e.g., Hancock et al., 2019). Of the three basins, the SJB was the most hydrographically restricted and likely experienced more water column stratification compared to the other two sites, which ultimately led to elevated sulfide production and preservation of pyrite (e.g., Hancock et al., 2019). Although these basins were predominantly anoxic and sometimes eu-



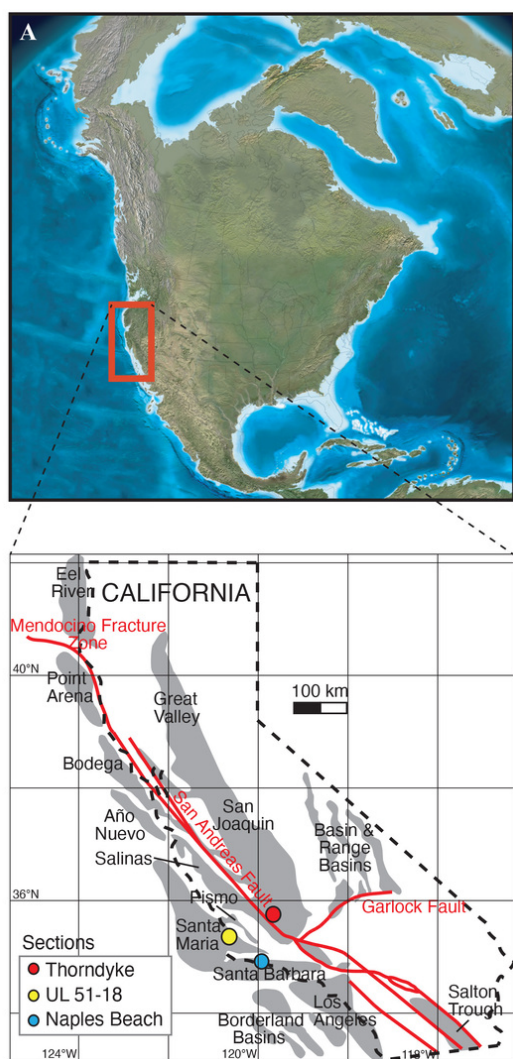


**Figure 2. Paleogeography and study sites. A) Paleogeography of North America during the Miocene (modified from Blakey, 2014). B) Neogene basins and study site locations (modified from Hancock et al., 2019).**

xinic (e.g., Hancock et al., 2019), there is minimal evidence that any of them were restricted to the degree of the Black Sea. Instead, they maintained strong connections with Pacific Ocean water and were saline throughout the entire water column.

## 5. MATERIALS AND METHODS

### 5.1. Mercury concentrations

Splits of samples from a previous study of the MMF (e.g., Hancock et al., 2019) were analyzed for Hg concentrations in the Geochemistry of Ancient and Modern Environmental Systems (GAMES) Laboratory at the College of Charleston in spring, 2019. Approximately 25–100 mg of sample powder were added to a nickel boat and placed into a Milestone DMA-80 evo rapid mercury analyzer and heated in stages to 750 °C. Volatilized Hg was collected by gold amalgamation before being measured via spectral analysis. All sam-

ples contained quantifiable Hg concentrations. A serial dilution of a 1,000-ppm ICP-MS Hg solution (Ricca Chemical Company) was used to calibrate the machine, and day-to-day calibrations were performed using international reference standards (TORT-3 SRM and DORM-4 SRM), which bracketed the full range of Hg concentrations calculated in these geologic samples. For the TORT-3 and DORM-4 standards, the average values and errors were  $293.4 \pm 9.7$  ng/g ( $N = 66$ ) and  $406.2 \pm 10.4$  ng/g ( $N = 53$ ), respectively, which show a narrower range of variance compared to their reported values ( $292 \pm 22$  and  $412 \pm 36$  ng/g, respectively). The average error in Hg concentrations is 2.3 ng/g (range of 0–19.0 ng/g, 15% of samples replicated at least once) for the Thorndyke core; 9.3 ng/g (range of 0.1–41.4 ng/g, 21% of samples replicated at least once) for Union Leroy; and 1.0 ng/g (range of 0–2.4 ng/g, 13% of samples replicated at least once) at Naples Beach. Analytical blanks were always  $< 0.5\%$  of the total Hg compared to the subsequent sample when measured. To ensure minimal contamination between samples, samples were always duplicated if the previous sample contained significantly elevated Hg concentrations.

### 5.2. Total sulfur and pyrite concentrations

Select samples from the study of Hancock et al. (2019) were analyzed and/or re-analyzed for total sulfur and/or pyrite contents. Some of these samples contained uncharacteristically high Hg concentrations (e.g., some of the highest shown for the Phanerozoic; see Grasby et al., 2019), and it was therefore necessary to rule out the accumulation of other host phases that may have resulted in their Hg enrichments (e.g., see Shen et al., 2020).

Total sulfur (TS) and pyrite sulfur ( $S_{\text{pyr}}$ ) were measured at the University of California, Riverside. Total sulfur was measured via combustion on an Eltra CS-500 carbon-sulfur analyzer, with a precision better than 0.07 wt.%. The chromium reduction method (Canfield et al., 1986) was used to evolve hydrogen sulfide ( $\text{H}_2\text{S}$ ) from S bound to pyrite. A silver nitrate trap solution was used to precipitate the liberated  $\text{H}_2\text{S}$  as silver sulfide ( $\text{Ag}_2\text{S}$ ), which was then quantified gravimetrically and used to calculate  $S_{\text{pyr}}$  as a wt.%. Values from duplicate analyses were within 3% or better. Pyrite contents were calculated stoichiometrically from the  $\text{Ag}_2\text{S}$  values.

### 5.3. Organically bound sulfur

Organic matter may also represent an important sink of S in modern and ancient OM-rich marine sediments (Raven et al., 2015, 2018; Werne et al., 2003), and thus its contribution should be further studied. We estimated the amount of organically bound sulfur by subtracting  $S_{\text{pyr}}$  from TS;  $S_{\text{pyr}}$  and TS were previously measured by Hancock et al. (2019) and some were measured for this study:

$$\text{Organic sulfur} = \text{TS} - S_{\text{pyr}} \quad (1)$$

Note, due to small errors on the TS and CRS methods (up to ~0.1 wt. %), six samples from Naples Beach contained organic sulfur values that were slightly negative; an organic

sulfur value of 0% was used for these samples during subsequent statistical analysis.

#### 5.4. Maximum temperature ( $T_{\max}$ )

A maximum temperature estimate ( $T_{\max}$ ), used to assess thermal maturity, represents the temperature at which the maximum amount of hydrocarbons is produced.  $T_{\max}$  data for select Santa Maria Basin (Union Leroy 51-18 drill core) samples were determined by Rock-Eval pyrolysis, conducted by GeoMark Research Ltd., Houston Texas. Previous research suggests that MMF sediments range from thermally immature to mature (e.g., Pytte, 1989; Rahman et al., 2017).

## 6. RESULTS

To be consistent with previous research on these cores, we continue to use the geochemical/sedimentological subdivisions identified based on other integrated datasets (see Hancock et al., 2019) that are included in the main figures for each study site.

### 6.1. San Joaquin Basin, Thorndyke 882-D-8 drill core

Results from SJB are shown in [figure 3](#). Mercury concentrations range from ~6 to 350 ng/g ( $N = 183$ ). In the SJB1 interval (3860–3820 m), Hg concentrations show an overall decreasing trend with a few anomalies from 3845–3830 m. In the SJB2 interval, Hg concentrations display similar concentrations relative to the lower SJB1 interval. In the SJB3 interval, Hg concentrations remain relatively invariant and similar in magnitude to the upper SJB1 interval. In general, the Hg concentrations are enriched relative to average sedimentary rock (62.4 ng/g including shale, sandstone, and limestone; e.g., Grasby et al., 2019). The only anomalous Hg/TOC values occur in the SJB1 interval, which also shows several Hg/TS, Hg/ $S_{\text{pyr}}$ , and Hg/Al anomalies. There are also no Hg or Hg/TOC anomalies in the volcanic ash layers.

### 6.2. Santa Maria Basin, Union Leroy 51-18 drill core

Results from SMB are shown in [figure 4](#). Mercury concentrations range from ~14 to ~1751 ng/g ( $N = 102$ ) and have elevated values in the lowermost section (~1480–1465 m) but remain relatively lower and invariant through the remainder of the section. The Hg concentrations are significantly enriched relative to the sedimentary rock average (e.g., Grasby et al., 2019). The only elevated and anomalous Hg/TOC values occur scattered in the SMB1 interval, and each is associated with elevated Hg/TS, Hg/ $S_{\text{pyr}}$ , or Hg/Al values ([fig. 4](#)). Last, the  $T_{\max}$  values from select samples within this core range from 390–416 °C (see [table 1](#)).

### 6.3. Santa Barbara Basin, Naples Beach section

Results from SBB are shown in [figure 5](#). Mercury concentrations range from ~27 to 210 ng/g ( $N = 139$ ). These concentrations show a decreasing trend from the base of the section to ~35 m, increase to ~85 m, and then decrease again and remain relatively constant up to a few elevated values

near the top of the section. In general, the Hg concentrations are enriched relative to the sedimentary rock average, but there are no anomalous Hg/TOC values compared to the Phanerozoic average (see Grasby et al., 2019), although some elevated values are apparent in the lower portion of the section. There are several relative Hg/TOC, Hg/ $S_{\text{pyr}}$ , and Hg/Al enrichments scattered throughout the stratigraphy, but these intervals do not correspond with one another. A step-change in the average Hg/Al value occurs around 85 meters, where the average Hg/Al value decreases from ~430 (ng/g)/wt% to ~210 (ng/g)/wt%.

## 7. DISCUSSION

### 7.1. Evaluating the controls on Hg sequestration in the Monterey Formation

One of the main assumptions of the Hg proxy is that sedimentary Hg enrichments are driven by increased Hg loading, typically from enhanced atmospheric deposition of volcanic-derived Hg, on a global scale. We find that enrichment can instead reflect specific depositional environments within a basin that enhance the accumulation and preservation Hg in sediments. In each basin of the MMF that we studied, there was likely a different primary control on Hg accumulation. In this section, we will discuss the mechanism(s) controlling Hg deposition at each location.

#### 7.1.1. SAN JOAQUIN BASIN (SJB), THORNDYKE 882-D-8 DRILL CORE

This drill core site, situated in the southern region of the basin ([fig. 2](#)), is the most proximal to the North American continent. Accordingly, the strongest relationships in the entire population of data, although weak, are between Hg and  $S_{\text{pyr}}$  ( $r^2 = 0.25$ ) as well as aluminosilicate ( $r^2 = 0.16$ ) contents ([fig. 6](#)), the latter reflecting detrital inputs from continental runoff. There is effectively no relationship with TOC for the entire core ( $r^2 = 0.06$ ). Although weak to moderate, these relationships suggest detrital sources of Hg and subsequent, possibly diagenetic, uptake due to local redox conditions (i.e., sulfide formation and burial). It has recently been suggested for samples with TOC > 1% and TS/TOC > 0.35 that Hg is likely hosted by sulfide (Shen et al., 2020). The relationship between Hg and  $S_{\text{pyr}}$  weakens in our entire sample population above those thresholds ( $r^2 = 0.043$ ,  $N = 31$ ; see section 7.1.4).

An increase in  $\text{Fe}_T/\text{Al}$  values and Mo concentrations, both proxies for local redox conditions, occurs in the transition between SJB1 and SJB2 (see Hancock et al., 2019). If we view these data within the context of the pre-established geochemical subunits defined in part by Fe and Mo data, then we start to see logical and consistent patterns. For example, in the SJB1 interval, Hg and pyrite are more strongly correlated ( $r^2 = 0.41$ ) than Hg and Al ( $r^2 = 0.16$ ) and Hg and TOC ( $r^2 = 0.06$ ). Using the thresholds from Shen et al. (2020) to determine samples that are controlled by local redox, the correlation between Hg and pyrite is weak ( $r^2 = 0.06$ ;  $N = 9$ ), which is less than both the entire population

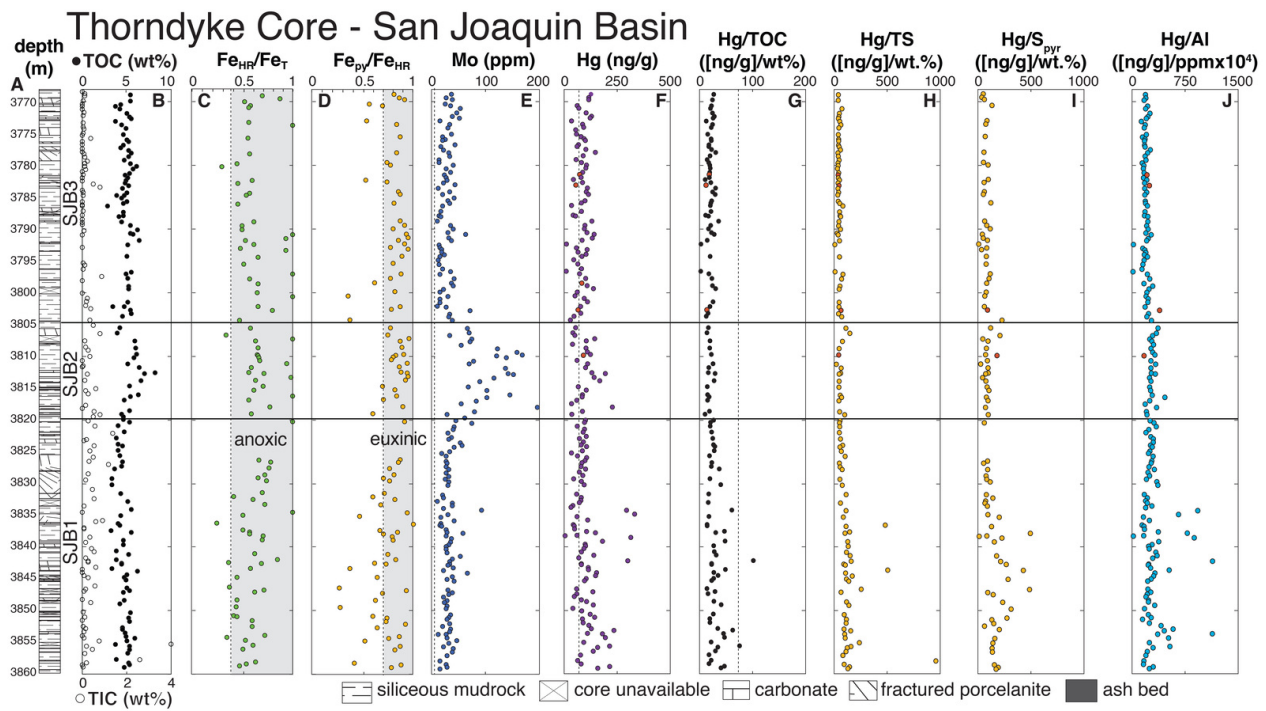


**Figure 3. Geochemistry of the Thorndyke 882-D-8 drill core (SJB).** Lithological, carbon, sulfur, iron, molybdenum, and aluminum data from Hancock et al. (2019). Mercury and some sulfur concentration data are from this study. Note, samples collected from within ash layers are colored red. The iron speciation data in columns C and D detail sedimentation under oxic or anoxic environments and ferruginous or euxinic environments, respectively (see Hancock et al., 2019 for full explanation of this proxy). Vertical dashed lines in columns F and G represent the Phanerozoic sedimentary rock averages (e.g., Grasby et al., 2019).

**Table 1. Mean concentration or ratio with one standard deviation for specific geochemical indices.**

Site	T <sub>max</sub> (°C)	Hg (ng/g)	TOC (wt. %)	Hg/TOC	S <sub>pyr</sub> (wt. %)
Naples Beach outcrop	401–417*	89.45 ± 40.59	8.84 ± 4.61	10.83 ± 3.64	1.21 ± 0.91
Thorndyke 882-D-8 drill core	435–440**	98.29 ± 50.69	4.17 ± 0.91	24.83 ± 12.86	0.50 ± 0.32
Union Leroy 51-18 drill core	390–416***	311.64 ± 252.21	8.10 ± 4.88	51.78 ± 64.97	0.60 ± 0.40

\* Rock-Eval data from unweathered Carbonaceous Marl member (Katz & Royle, 2001)

\*\* Rock-Eval data from Curiale and Odermatt (1989) and Barnette (2015)

\*\*\* Rock-Eval data from *this study*

of data and the SJB1 interval. Mercury is more likely to be associated with pyrite burial in SJB1.

In the SJB2 interval, Hg and pyrite are moderately correlated ( $r^2 = 0.54$ ) compared to SJB1, with strong correlations between Hg and Al ( $r^2 = 0.82$ ) and Hg and TOC ( $r^2 = 0.65$ ). The removal of one sample point (3811.19 m) with an anomalously high pyrite concentration from SJB2 significantly increases the Hg-pyrite relationship ( $r^2 = 0.78$ ). The removal of this data point does not affect the Hg-Al relationship and only slightly increases the Hg-TOC relationship ( $r^2 = 0.68$ ). There is a strong correlation between pyrite and Al in this subdivision ( $r^2 = 0.67$ ) when the sample at 3811.19 m is removed ( $r^2 = 0.41$  in entire SJB2 dataset), pointing to an association between the formation/burial of pyrite and potentially to changes in clay mineral content, which may have affected permeability of the sediments and subsequent diagenetic processes. Oddly enough, this correlation does not exist in SJB1 ( $r^2 = 0.06$ ) where Hg and

pyrite are the only variables with a moderate correlation. Using the thresholds for a sulfide host phase from Shen et al. (2020) for sample filtering, the correlation between Hg and pyrite, however, is slightly higher than for SJB1 ( $r^2 = 0.16$ ;  $N = 6$ ). This Hg-pyrite relationship increases dramatically if one sample point (3811.19 m) is removed ( $r^2 = 0.99$ ). In general, Hg is likely associated with pyrite burial in SJB2, but other host phases such as clays and organic matter may also be important on a sample-specific level.

In SJB3, Hg and TOC are weakly correlated ( $r^2 = 0.18$ ), with increasing correlations between Hg and Al ( $r^2 = 0.35$ ) and Hg and pyrite ( $r^2 = 0.53$ ). If one sample at 3792.44 m is removed (abnormally low Hg concentrations), then the Hg and pyrite relationship increases significantly ( $r^2 = 0.72$ ). If two samples at 3792.44 m and 3796.71 m (another sample with abnormally low Hg concentrations) are removed, then the Hg and Al relationship increases significantly ( $r^2 = 0.73$ ), as does the Hg and TOC relationship ( $r^2 = 0.30$ ); there



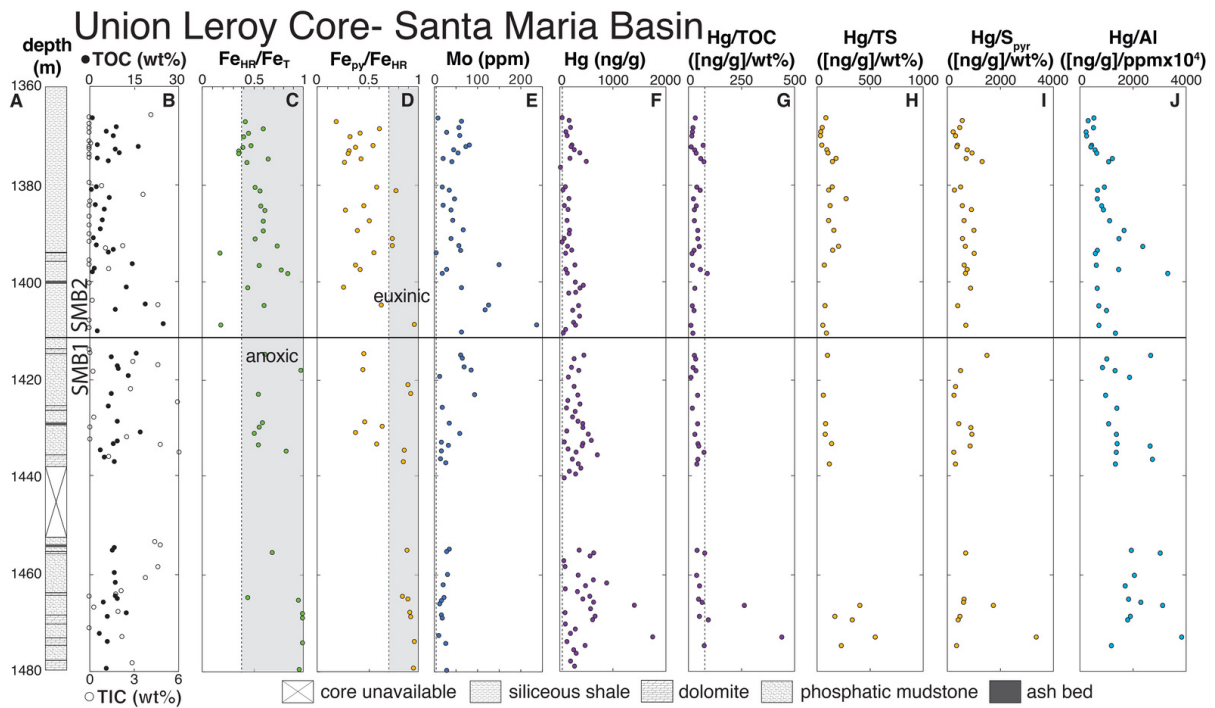


**Figure 4. Geochemistry of the Union Leroy 51-18 drill core (SMB).** Lithological, carbon, sulfur, iron, molybdenum, and aluminum data from Hancock et al. (2019). Mercury and some sulfur concentration data are from this study. Vertical dashed lines in columns F and G represent the Phanerozoic sedimentary rock averages (e.g., Grasby et al., 2019).

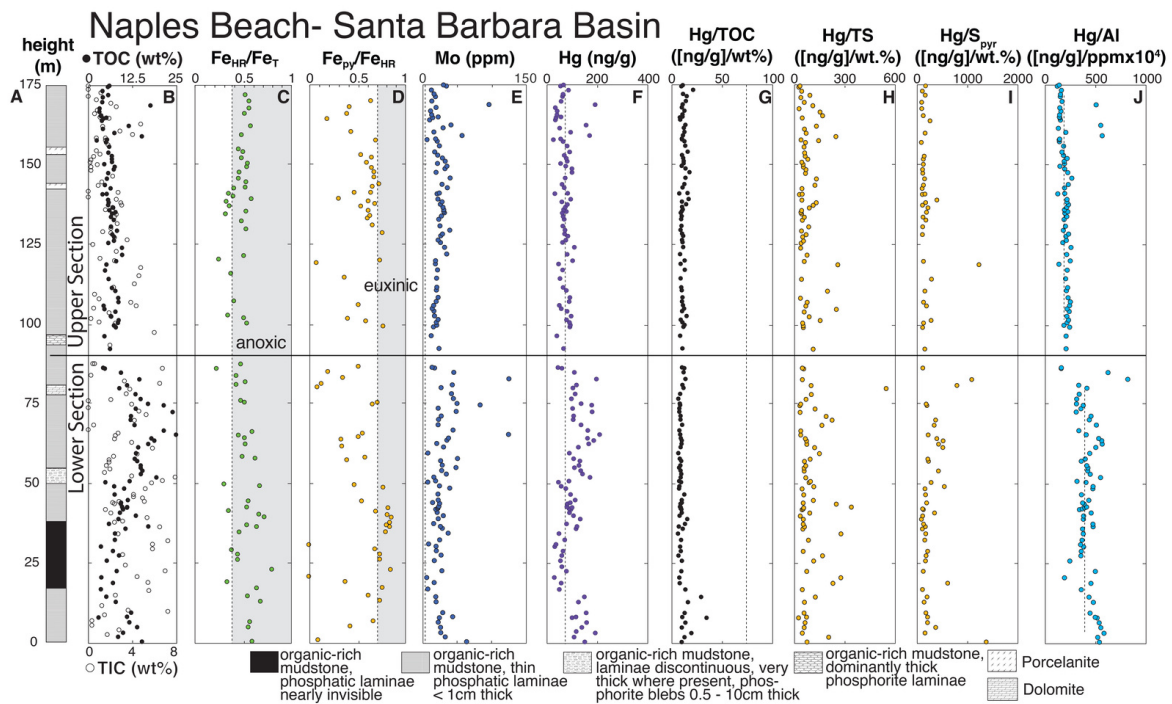


**Figure 5. Geochemistry of the Naples Beach section (SBB).** Lithological, carbon, sulfur, iron, molybdenum, and aluminum data from Hancock et al. (2019). Mercury and some sulfur concentration data are from this study. Vertical dashed lines in columns F and G represent the Phanerozoic sedimentary rock averages (e.g., Grasby et al., 2019).

is no pyrite datum for 3796.71 m. Considering the Shen et al. (2020) thresholds in SJB3, Hg and pyrite are moderately correlated ( $r^2 = 0.29$ ,  $N = 16$ ), but this correlation increases

significantly if the same data point at 3792.44 m is removed ( $r^2 = 0.74$ ). Mercury is likely associated with pyrite burial in SJB3, but a clay mineral host phase is also apparent. The



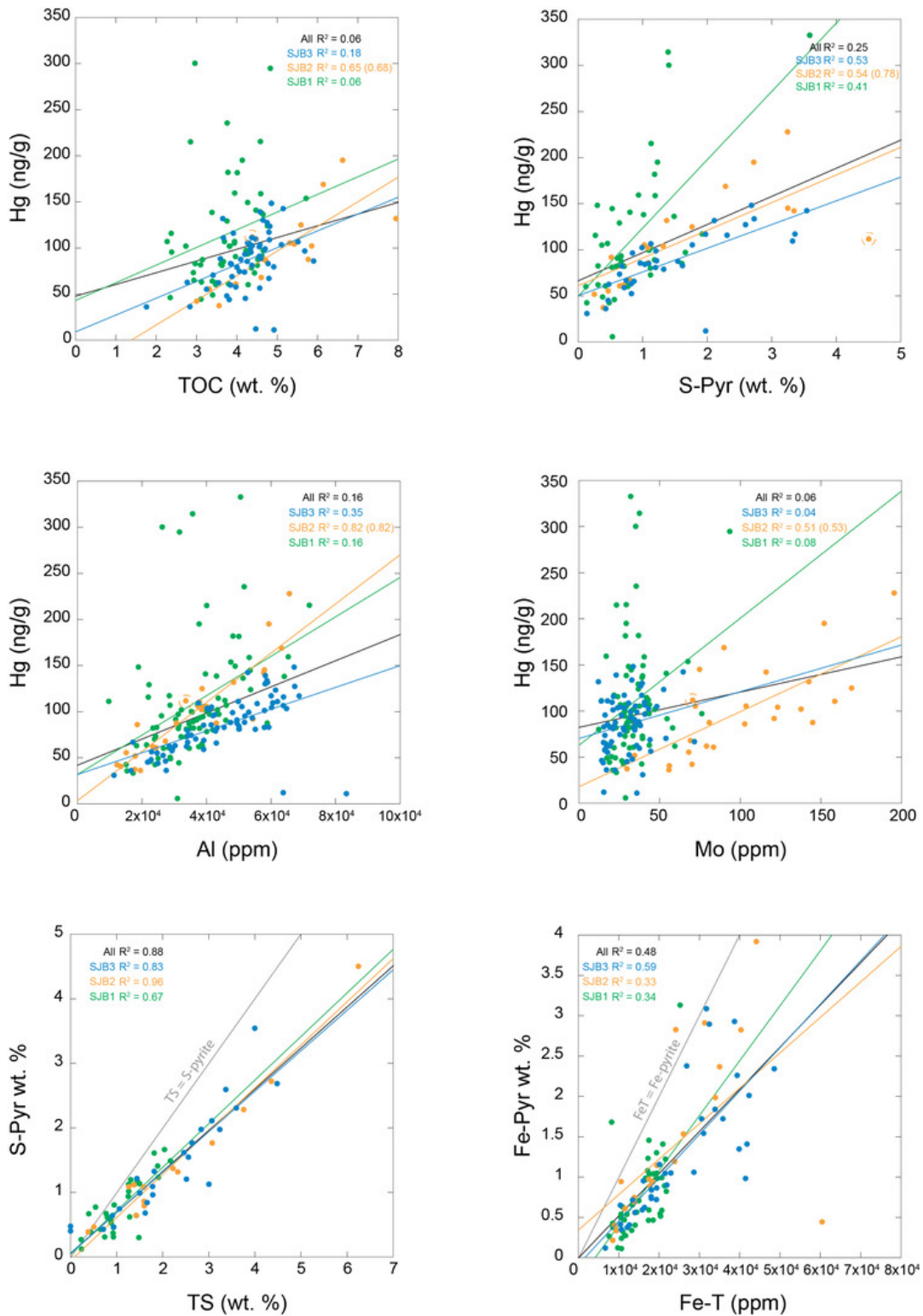


**Figure 6. Geochemical relationships in the Thorndyke 882-D-8 drill core (SJB).** Basic cross-plots between Hg and TOC, S-pyrite, Al, and Mo, as well as between S-pyrite and TS and Fe-pyrite and Fe-T. Gray line in the  $S_{pyr}$ :TS and  $Fe_{pyr}$ :Fe-T graphs represents the 1:1 relationship between the geochemical parameters; data points below this line represent samples where TS or Fe-T values overestimate the amount of pyrite. Data are from Hancock et al. (2019) and this study. Note, the  $r^2$  value in parentheses is the value when the circled data point is removed from statistical analysis as discussed in the main text.

moderately strong correlation between pyrite and Al ( $r^2 = 0.60$ ) also points to an association between the formation/burial of pyrite and clay mineral content, similar to that

observed in SJB2. It is clear from the statistical analyses within the subunits in this core that single data points have

the potential to alter the relationships in the entire population and therefore any subsequent interpretations.

The slightly elevated Hg enrichments in the middle of the SJB2 interval are associated with a shoaling of the sulfidic conditions into the highly stratified water column (e.g., euxinia), likely facilitating metal removal, especially Mo, into sediments (e.g., Hancock et al., 2019). Considering the more muted Hg enrichments in SJB2 relative to Mo, it seems plausible that Hg accumulation was limited by the flux of Hg into the basin potentially due to limited physical mixing of the water column. The strong relationship between Hg and Al supports a proximal, terrestrially derived Hg source that does not require a well-mixed water column to increase Hg accumulation. Although the formation and burial of pyrite along with different contributions of Hg transported via detrital minerals were likely the dominant mechanisms that led to the accumulation of Hg during the entire SJB study interval, there are clear temporal variations that are likely associated with the overall redox regime and position of the chemocline within the basin.

### 7.1.2. SANTA MARIA BASIN, UNION LEROY 51-18 DRILL CORE

Approximately 100 km to the southwest of SJB (fig. 2), multiproxy data also suggest numerous processes controlling Hg deposition in the SMB over the interval of interest. The strongest relationships with Hg, although weak, are with pyrite ( $r^2 = 0.15$ ) and aluminosilicate ( $r^2 = 0.13$ ) content (fig. 7). There is effectively no relationship with TOC for the entire core ( $r^2 = 0.02$ ). There are two samples, however, with elevated Hg concentrations that skew these statistics (1466.39 and 1472.89 m). If these two samples are removed from the basic statistical analysis, then the correlations dramatically improve. The strongest correlation, as for the entire SMB dataset, is between Hg and pyrite ( $r^2 = 0.49$ ), but the Hg and TOC correlation also strengthens relative to the entire SMB dataset ( $r^2 = 0.22$ ). The correlation with Hg and Al remains unchanged relative to the entire SMB dataset ( $r^2 = 0.13$ ; fig. 7). The dominant host phase for Hg appears to be pyrite, with organic matter exerting a subordinate control on Hg accumulation in the Santa Maria Basin.

In samples where we would expect Hg to be hosted in sulfide based on basic TS/TOC and TOC thresholds, we instead find no correlation between Hg and  $S_{\text{pyr}}$  ( $r^2 = 0.02$ ,  $N = 11$ ; see section 7.1.4; see Shen et al., 2020). This result is similar to the trends observed from SJB and opposite of what is expected if this threshold is indicative of Hg sequestration into sulfide minerals. If the two samples with anomalous Hg concentration values are removed from this analysis, then the correlation increases slightly ( $r^2 = 0.14$ ,  $N = 9$ ) but is still much lower than the relationship using the full SMB dataset.

Other patterns in the data are apparent when dividing SMB into SMB1 and SMB2 intervals. In SMB1, the Hg to TOC ( $r^2 = 0.08$ ) and Hg to pyrite ( $r^2 = 0.04$ ) correlations are both weak, yet the Hg to Al correlation is moderate ( $r^2 = 0.44$ ). Excluding the two data points with elevated Hg concentrations only slightly alters these correlations. The Hg

and TOC ( $r^2 = 0.05$ ) and Hg and pyrite ( $r^2 = 0.03$ ) correlations are still both weak, and the Hg and Al correlation also weakens, but remains moderate ( $r^2 = 0.33$ ). Here, the pyrite to Al correlation is also weak ( $r^2 = 0.07$ ). In the SMB2 interval, the Hg and TOC ( $r^2 = 0.39$ ), Hg and pyrite ( $r^2 = 0.31$ ), and Hg and Al ( $r^2 = 0.48$ ) correlations are all moderate. Interestingly, the removal of one data point (1375.56 m) with an elevated Hg concentration alters these correlations, such that the Hg and TOC relationship ( $r^2 = 0.55$ ) is higher than both Hg and Al ( $r^2 = 0.53$ ) and Hg and pyrite ( $r^2 = 0.42$ ). The pyrite to Al correlation increases significantly in SMB2 ( $r^2 = 0.59$ ) in association with a transition between clay minerals in SMB1 and organic matter/sulfide in SMB2 as the dominant host phase(s). The correlation between Hg and pyrite also changes significantly when the thresholds of Shen et al. (2020) are used in the subdivisions. For example, there is a moderate inverse correlation between Hg and pyrite ( $r^2 = 0.41$ ,  $N = 5$ ) in SMB1 and no correlation in SMB2 ( $r^2 = 0.01$ ,  $N = 6$ ). Oddly, when the two data points with high Hg concentrations are removed in SMB1, a stronger inverse correlation between Hg and pyrite ( $r^2 = 1$ ,  $N = 3$ ) is apparent. Subdividing the SMB data population places a greater emphasis on aluminosilicates (e.g., clay minerals) and organic matter as controlling the Hg cycle in the SMB1 and SMB2 intervals, respectively, which was not apparent in the full dataset.

### 7.1.3. SANTA BARBARA BASIN, NAPLES BEACH SECTION

Approximately 80 km southeast of SMB and 120 km south of SJB (fig. 2), multiproxy data suggest a straightforward host phase for Hg accumulation in the SBB during the study interval, despite varying transport mechanisms of Hg associated with detrital input. Specifically, a critical role played by organic matter is indicated by the strong Hg relationship with TOC ( $r^2 = 0.72$ ) and a lack of correlation with pyrite ( $r^2 = 0.10$ ) and Al concentrations ( $r^2 = 0.09$ ; fig. 8).

Although it is initially apparent that the dominant host phase in the SBB is organic matter, there are two clear populations of data in the Hg-Al cross plot that warrant closer inspection (fig. 8). In the lower half of the section (0–86.5 m), the Hg and Al correlation is much stronger ( $r^2 = 0.57$ ) compared to the upper half (92.4–175 m;  $r^2 = 0.18$ ; note, this relationship increases to  $r^2 = 0.53$  if three samples where Hg > 150 ng/g are excluded) but much stronger than for the entire population of data in the study interval ( $r^2 = 0.09$ ). Mercury delivery linked to detrital materials was ~50% less, or aluminosilicate concentrations were ~200% higher (Hg/Al = ~420 (ng/g)/wt% in lower half relative to Hg/Al = ~200 (ng/g)/wt% in upper half) within the study interval. Based on the Hg and Al chemostratigraphies, this trend is driven in part by both changes in Hg concentrations (decreased by ~40%) and Al concentrations (increased by ~35%) in the upper half relative to the lower half. If the Hg-TOC correlations are also divided into these two populations within the core (i.e., lower half and upper half), the data suggest an up-core shift from clay minerals to organic matter as the dominant host phase. Specifically, the Hg-to-TOC correlation in the lower half is weaker ( $r^2 = 0.61$ ) compared to the upper half ( $r^2 = 0.78$ ). These observations may alternatively reflect a relationship between organic matter

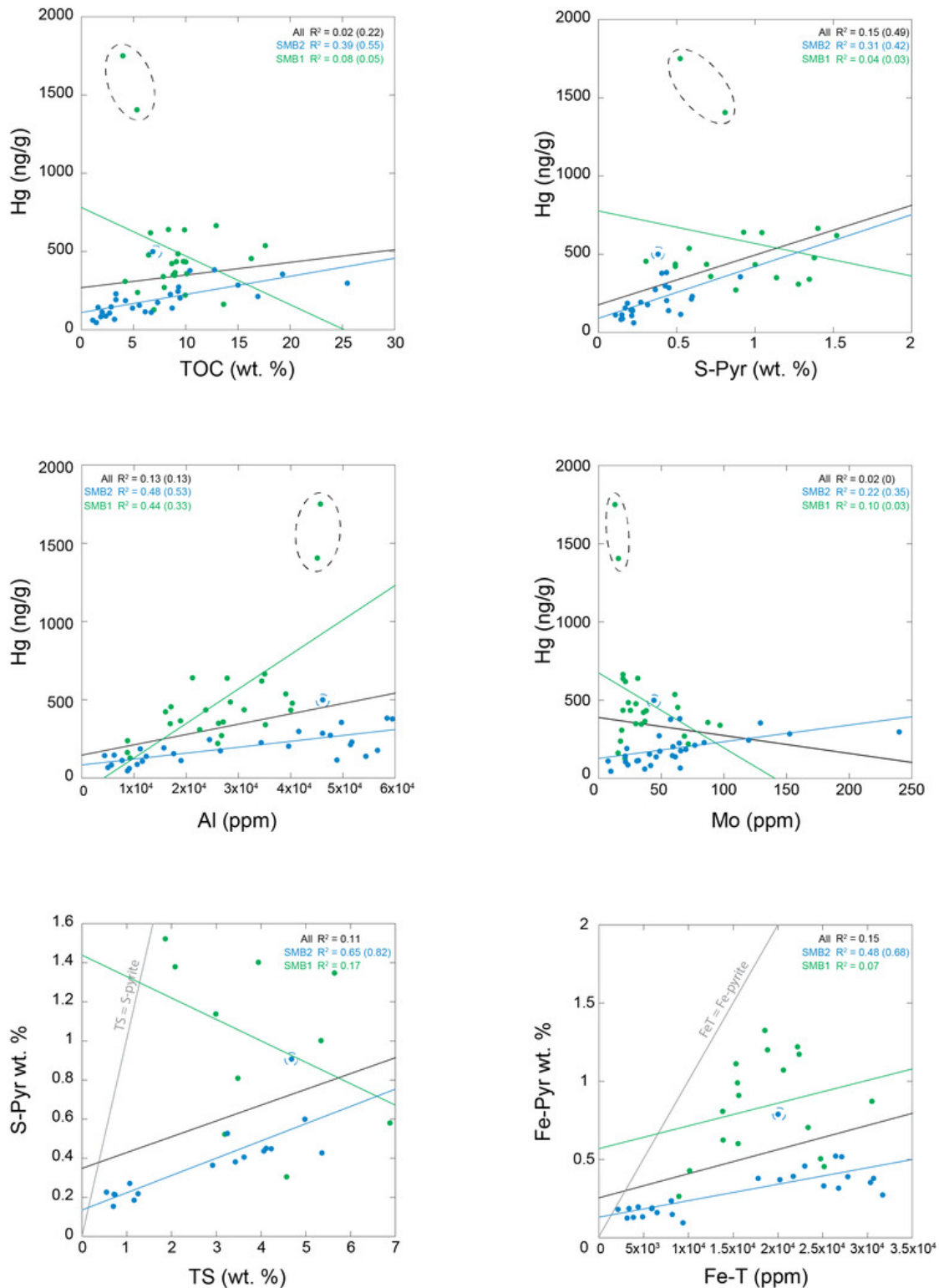


**Figure 7. Geochemical relationships in Union Leroy 51-18 drill core (SMB). Basic cross-plots between Hg and TOC, S-pyrite, Al, and Mo, as well as between S-pyrite and TS and Fe-pyrite and Fe-T. Gray line in the  $S_{\text{pyr}}:TS$  and  $Fe_{\text{pyr}}:Fe\text{-T}$  graphs represents the 1:1 relationship between the geochemical parameters; data points below this line represent samples where TS or Fe-T values overestimate the amount of pyrite. Data are from Hancock et al. (2019) and this study. Note, the  $r^2$  values in parentheses are the values when the circled data points are removed from statistical analysis as discussed in the main text.**

and detrital clay minerals (e.g., Hedges & Keil, 1995; Keil et al., 1994; Kennedy et al., 2002). The correlation between Hg and  $S_{\text{pyr}}$  decreases from the lower half ( $r^2 = 0.18$ ) to the

upper half ( $r^2 = 0.05$ ). It is important to note, however, that the Hg- $S_{\text{pyr}}$  correlation increases significantly if one anomalous data point (168.85 m) is removed in the upper half

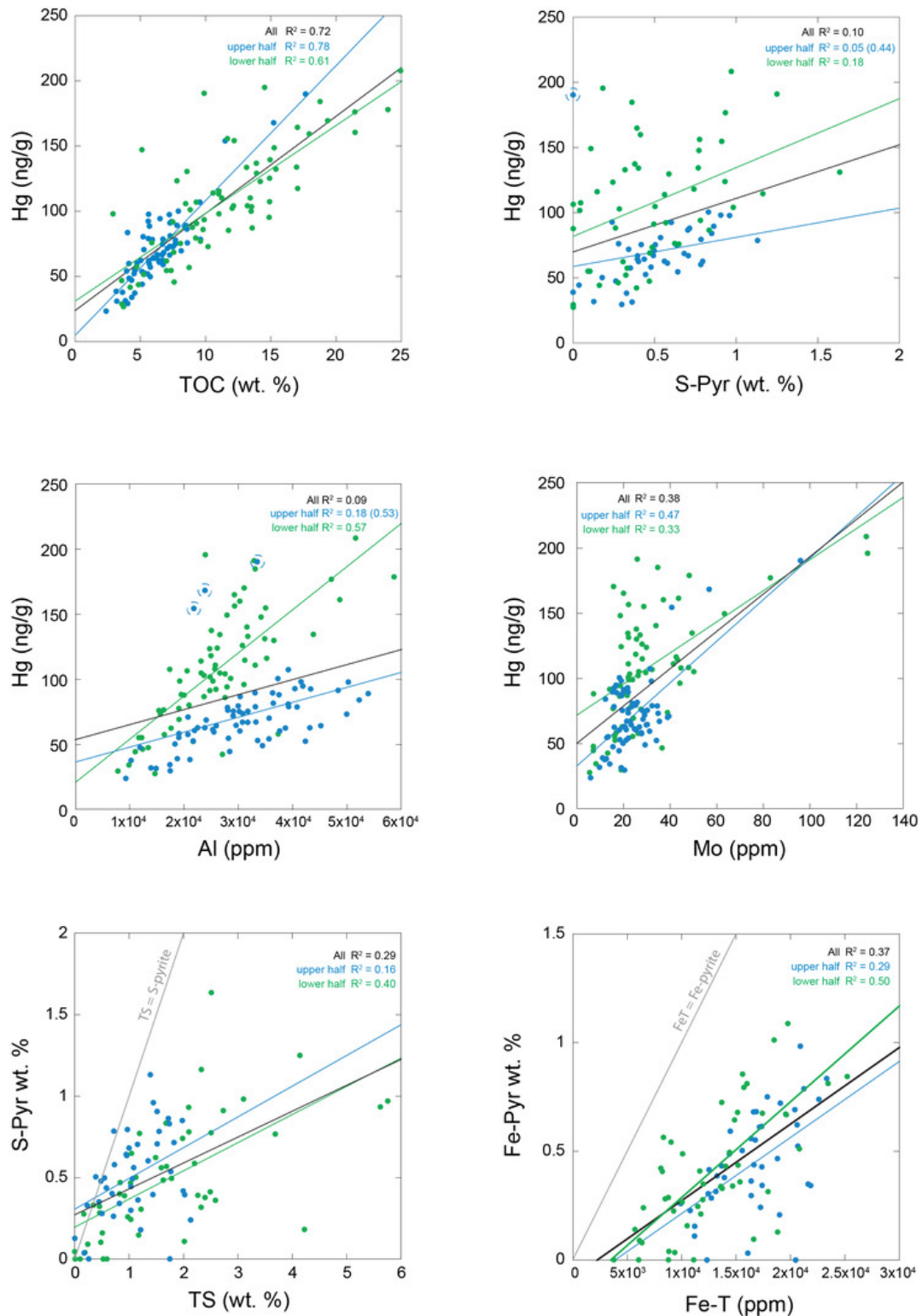


**Figure 8. Geochemical relationships in the Naples Beach section (SBB). Basic cross-plots between Hg and TOC, S-pyrite, Al, and Mo, as well as between S-pyrite and TS and Fe-pyrite and Fe-T. Gray line in the  $S_{pyr}$ :TS and  $Fe_{pyr}$ :Fe-T graphs represents the 1:1 relationship between the geochemical parameters; data points below this line represent samples where TS or Fe-T values overestimate the amount of pyrite. Data from Hancock et al. (2019) and this study. Note, the  $r^2$  values in parentheses are the values when the circled data points are removed from statistical analysis as discussed in the main text.**

( $r^2 = 0.44$ ; see [fig. 8](#)). The basic TS/TOC and TOC threshold used to determine whether Hg is hosted by sulfide (e.g., Shen et al., 2020) reveal that only a few data points suggest

dominance by a sulfide host, which is supported by the moderate Hg- $S_{pyr}$  correlation ( $r^2 = 0.50$ ,  $N = 3$ ).



Although organic matter was likely the most important host phase at Naples Beach based on the statistical relationships, the cycling of Hg would have been complicated by changes in detrital input and the production of sulfide and pyrite, which likely played dominant and subordinate roles, respectively. Furthermore, the covariations of Hg to Al could be a function of organic controls in combination with the strong affinity organic matter has for clay minerals (e.g., Hedges & Keil, 1995; Keil et al., 1994; Kennedy et al., 2002). Therefore, the strong Hg-to-Al relationship may not necessarily be indicative of a direct clay host phase in OM-rich facies, and further research will be required to disentangle these observations.

#### 7.1.4. TRADITIONAL SCREENING OF MERCURY CONCENTRATION DATA

Several methods are currently used to determine the most important factor controlling Hg accumulation in sediments other than organic matter loading (e.g., redox changes). As described above, threshold values for TS/TOC (>0.35) and TOC (>1%) have been suggested to explore redox-dependent controls on Hg accumulation (e.g., Shen et al., 2020; see fig. 9). This approach worked only at one of our three sites (SBB, where organic matter is likely the dominant host), but was also somewhat useful at the other two sites when anomalous data points were removed for reasons explained. There were caveats, as previously discussed, however, even at SBB that imply the cycling of sulfide was, during certain intervals, likely associated in Hg accumulation and burial, even though it was not apparent using the threshold. Furthermore, the contribution of organic sulfur to TS can be significant in modern and ancient sediments (e.g., Raven et al., 2015, 2018; Werne et al., 2003), which is observed in the MMF sediments. At Thorndyke, the range for the organic sulfur contribution to TS was 0–80% (average of 35%, median of 35%, N = 62); at Union Leroy, the contribution ranged from 18–93% (average of 77%, median of 83%, N = 27); and at Naples Beach, the contribution ranged from 0 to 100% (average of 57%, median of 60%, N = 92). These data confirm that use of TS to estimate the contribution of pyrite to any given sediment sample can be erroneous because much of the TS is present as sulfurized organic matter (as discussed in Grasby et al., 2019; Shen et al., 2020). Furthermore, we must also consider the possibility that Hg initially scavenged by sulfide minerals can be released back to the water column or pore waters during subsequent sulfide oxidation, followed by sequestration by organic matter or other mineral phases. Although these basins were predominantly reducing (e.g., Hancock et al., 2019), it is likely that transient intervals of oxygen penetration into the water column or sediments occurred. This recycling is difficult to resolve but may represent an important syn- or post-depositional mechanism to enrich ancient sediments in Hg relative to TOC, as OM is degraded or consumed during aerobic or anaerobic respiration (Frieling et al., 2023). Although methylation of Hg under reducing conditions may result in the evasion of Hg from the sediments into the water column (Frieling et al., 2023; Mason et al., 2006), the anoxic and sometimes euxinic nature of the MMF

deposits likely led to reduced loss due to the formation and burial of syngenetic pyrite, which would have represented an efficient scavenging mechanism.

In an important review of the sedimentary Hg proxy, Grasby et al. (2019) suggested distinct regions of log-log plots (Hg and TOC) to determine when sulfide-related uptake of Hg became the dominant mechanism to sequester Hg (fig. 9). This process is thought to occur because the increased fluxes of Hg to the environment during LIP emplacement overwhelm the ability of OM to sequester Hg, thus leading to the additional removal via sulfide (e.g., Grasby et al., 2019). Of the 424 Hg data points presented in our study, no samples plot in the sulfide uptake zone, even though it is clear from our cross plots that sulfide played a key role in Hg accumulation in a large proportion of samples (fig. 9). Grasby et al. (2019) relied on the assumption that TS is indicative of wt.%  $S_{\text{pyr}}$ , which is often not the case as discussed above. What is still not known, however, is whether free sulfide in the water column or sediments increases the particle reactivity of Hg, resulting in greater uptake by organic matter in the environment, thus complicating the Hg-TOC correlations. An Hg study from a meromictic lake does point to significant variation in Hg species related to local redox changes and the cycling of sulfur and iron (Tisserand et al., 2022), so it is likely that similar processes would also occur in a marine setting with similar redox processes in the water column or sediments. This mechanism (changes in particle reactivity) has been suggested as a critical process for the accumulation of another redox-sensitive element, Mo, in sulfidic settings (Algeo & Lyons, 2006; Chappaz et al., 2014; Erickson & Helz, 2000; Scott et al., 2008).

#### 7.1.5 DIRECT AND INDIRECT PROXIES FOR ROLE OF PYRITE IN MERCURY ACCUMULATION

Other common methods used to rule out a redox control for sedimentary Hg enrichments (e.g., as related to sulfide) rest on measurements of TS, FeT, and/or Mo concentrations (e.g., J. Chen et al., 2023; Fendley et al., 2024; Grasby et al., 2019; Kalvoda et al., 2019; Kovács et al., 2020; Y. Liu et al., 2023; Z. Liu et al., 2021; Pippenger et al., 2023; Ruhl et al., 2020; Shen et al., 2020). Pyrite concentrations can be measured directly though, for example, by using the chromium reduction technique (e.g., Canfield et al., 1986). Most studies, however, have not adopted that approach and therefore the utility of these alternative methods demands discussion. These other data are used indirectly as a proxy for pyrite concentrations or local redox conditions, which may help in assessments of whether Hg accumulation was related to pyrite burial. In the MMF, comparisons of  $S_{\text{pyr}}:TS$ ,  $Fe_{\text{pyr}}:FeT$ , and Hg:Mo yield overall weak trends (figs. 6–8), with a stronger correlation between  $S_{\text{pyr}}$  and TS at SJB and in the SMB2 subdivision. The contribution of  $S_{\text{pyr}}$  to TS concentrations may be overestimated because, in some circumstances, organic sulfur may represent a significant contributor (see earlier discussion).

Total iron values are commonly used to assess the contribution of pyrite in any given sample. Similar to  $S_{\text{pyr}}$  and TS,  $Fe_{\text{pyr}}$  and FeT values may also not correlate with one

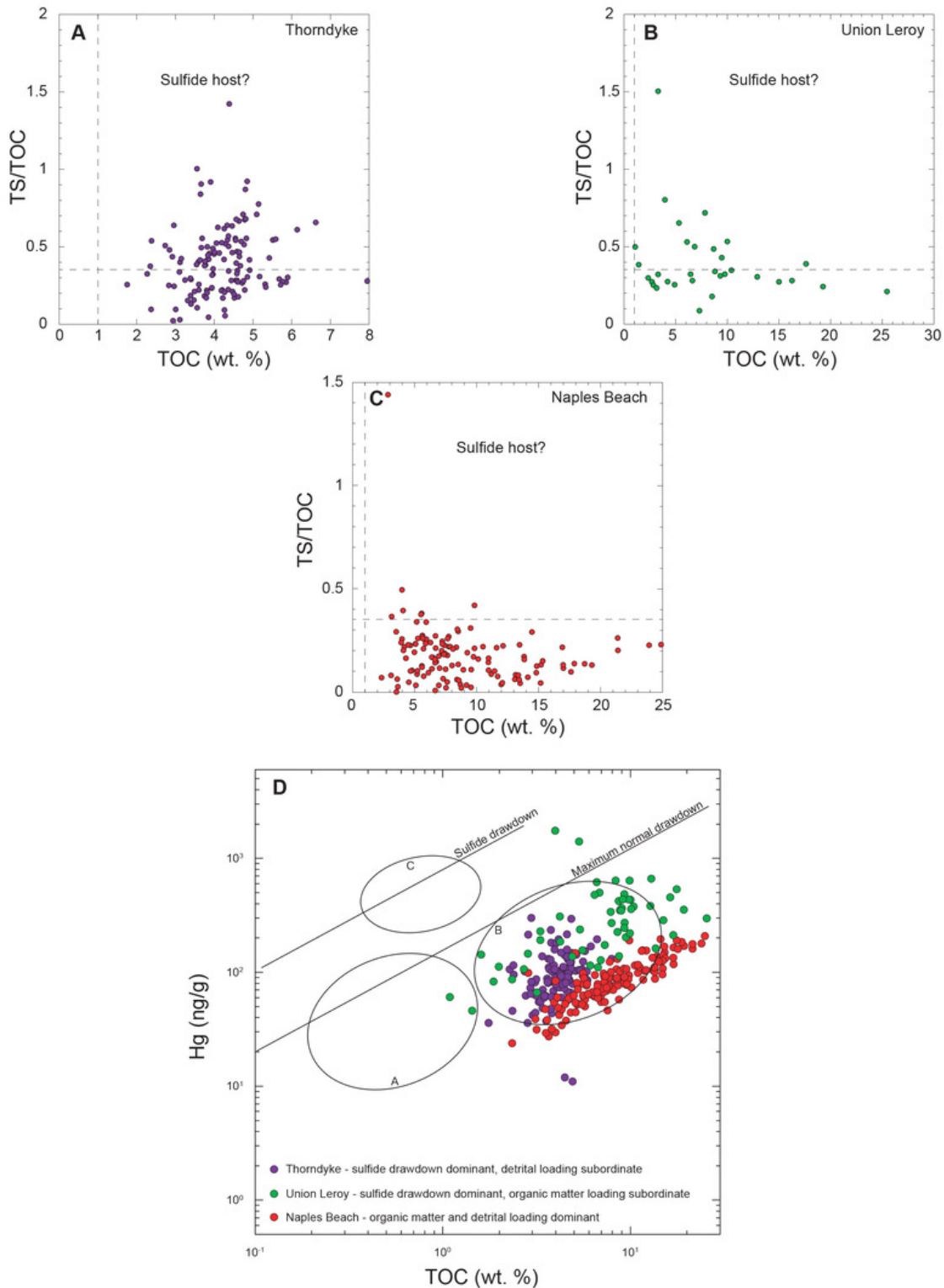


**Figure 9.** Assessment of standard methods for Hg sequestration in the MMF deposits. A, B, and C) Analysis of TS/TOC versus TOC to determine the role of sulfide using compilation by Shen et al. (2020). D) Analysis of organic matter versus sulfide drawdown using compilation by Grasby et al. (2019). Ellipses are from Grasby et al. (2013, 2019).

another because Fe can be delivered by multiple mechanisms such as detrital and/or aeolian processes, hydrothermal activity, or the precipitation of Fe-oxides on the seafloor or in the water column (e.g., Severmann et al., 2008). Issues with these relationships are apparent in the

datasets in this study (see [figs. 5–7](#)). FeT correlates with Fe<sub>pyr</sub> most commonly under euxinic conditions where FeT is elevated due to enrichments in reactive Fe and reactive Fe limitation overall (see Lyons & Severmann, 2006). Otherwise, under oxic conditions, where reactive Fe is often not

the limiting factor,  $Fe_{pyr}$  commonly scales with TOC (and thus sulfide-generating potential), with no effect on FeT. Therefore, FeT values may not scale directly with pyrite concentrations. Total Fe values consistently and significantly overestimate pyrite concentrations at all sites, but there is a strong correlation in the SMB2 subdivision (fig. 7).

The use of Mo concentrations to rule out a redox control on Hg (e.g., Z. Liu et al., 2021) is also fraught with issues. First, the range of Mo concentrations from fully oxygenated to euxinic environments can overlap below 25 ppm (e.g., Hardisty et al., 2018; Scott & Lyons, 2012, and references therein), potentially leading to erroneous interpretations of free sulfide availability for any given sample. Second, the global marine reservoir of Mo is sensitive to the geographic extent of anoxic and euxinic environments in the ocean (e.g., Owens et al., 2016; Scott et al., 2008; Them et al., 2022). For example, if the proportion of euxinic environments increases across a given time interval, then the Mo reservoir will decrease due to ubiquitous uptake in those euxinic basins, placing upper limits on the Mo concentrations that will be expected at any given location—even if deposition occurs in locally euxinic environments. Such drawdown of the global marine Mo inventory is not likely for the Miocene, as the studied euxinic sediments are strongly enriched in molybdenum (Hancock et al., 2019). It is likely, however, that the Mo reservoir was depleted across many of the ancient climatic events where the Hg proxy has been applied (e.g., Algeo, 2004; Owens et al., 2016; Them et al., 2022). Third, the main host phase of Mo in sediments may be organic matter rather than pyrite (e.g., Chappaz et al., 2014; cf. Gregory et al., 2015; Large et al., 2014). Molybdenum is rapidly sequestered in euxinic environments because it becomes particle reactive, which increases the scavenging efficiency by both organic matter and sulfides (e.g., Erickson & Helz, 2000; Scott et al., 2008; cf. Chappaz et al., 2014). In the MMF, the only site to have a moderate correlation between Hg and Mo was the upper half subdivision of Naples Beach ( $r^2 = 0.47$ ), and in this section Hg was also strongly correlated to TOC (fig. 8).

Based on this analysis, we suggest that the chromium reduction of sulfide (CRS) method should be used to measure pyrite concentrations in sediments (e.g., Canfield et al., 1986) rather than indirect methods such as TS, FeT, and/or Mo concentration data. If performed properly, this approach will ensure more accurate interpretations of the role of redox and pyrite in sedimentary Hg concentrations (e.g., Shen et al., 2019; Them et al., 2019). It should be noted, however, that a link between Hg and TOC at oxic sites could reflect direct uptake onto OM or high OM yielding high sulfide, which is important for diagenetic pyrite formation – with pyrite as the Hg host. Most importantly, these local variations in redox and OM cycling make it difficult to confidently ascribe changes in Hg concentrations solely to increased extra-basinal inputs such as volcanism.

## 7.2. Effects of burial history and weathering on Hg systematics

Both Hg and Hg/TOC values in sedimentary rocks have the potential to be affected by post-depositional processes such as heating during burial and weathering during subsequent exposure and oxidation (e.g., Charbonnier et al., 2020; D. Chen et al., 2022; Park et al., 2022). During weathering, whether incipient or extreme, pyrite minerals in sedimentary rocks are oxidized before organic matter (e.g., Petsch et al., 2000; Tuttle & Breit, 2009; Wildman et al., 2004). Precautions must be taken with regard to assessing the impacts of weathering before interpreting Hg geochemical records (e.g., Park et al., 2022). We do not find evidence that weathering impacted our geochemical records. Naples Beach is the only outcrop exposure, and therefore the only site expected to be impacted by incipient or extreme weathering (e.g., Charbonnier et al., 2020; Park et al., 2022). The weathering of pyrite can also occur in subsurface environments (Gu et al., 2020), but our drill cores do not show signs of appreciable pyrite oxidation. A comparison of our Naples data to the Thorndyke and Union Leroy drill cores reveals that differences in Hg and Hg/TOC values cannot be explained by weathering of pyrite or organic matter (see table 1). Naples Beach contains pyrite concentrations that are on average twice as high as both drill cores and TOC values that are also on average higher than both sites (see table 1). Furthermore, the samples collected from Naples contained no visual signs of oxidation associated with weathering, and Fe-oxide concentrations (a mineral product of sulfide weathering) are not elevated (Hancock et al., 2019). Furthermore, there is no evidence for diagenetic imprinting from recent fluid-rock interactions over the last 1 Myr on uranium isotopes from the Naples Beach section (Lau et al., 2022).

Increased heating and pressure may affect Hg and Hg/TOC records (D. Chen et al., 2022). In laboratory experiments, a modern soil and powdered black shale that experienced Hg loss were dependent on two factors: 1) host phase and 2) temperature-pressure gradients. Mercury associated with organic matter was volatilized rapidly after temperatures increased above 250 °C, whereas Hg associated with clay minerals was volatilized only after temperatures increased above 400 °C (D. Chen et al., 2022). The MMF rocks did not reach these extreme temperatures or pressures during their burial history. Temperatures and pressures that approach those leading to metamorphic grade overprints show clear evidence that the Hg system can be affected (D. Chen et al., 2022). Our Hg and TOC data (or any of the other datasets), however, do not covary in a systematic way with  $T_{max}$  values for any of the sites studied in the MMF (see table 1). Based on the datasets we present and the burial history of each site, there is no compelling evidence for post-depositional alteration of the original paleoenvironmental signals (e.g., Hancock et al., 2019; Lau et al., 2022). It is important to note that the laboratory data from D. Chen et al. (2022) were focused on black shales rather than highly siliceous, organic-rich lithologies like those observed in the MMF sediments. We suggest that future experiments that focus on similar lithologies are warranted to

determine if and how diagenetic processes impact the Hg properties of sediments with different permeabilities.

### 7.3. Possible sources of Hg to the eastern Pacific Ocean

There are many possible mechanisms to deliver, transport, and sequester Hg in the natural environment (see Grasby et al., 2019). In marginal marine environments, it is likely that Hg delivery is dominated by sources of Hg from land or an advecting water mass (e.g., M. Liu et al., 2021); atmospheric deposition of Hg is likely a subordinate mechanism. The MMF locations studied give us a range of calibration points to test these possible delivery pathways since they span isolated (e.g., SJB) to open ocean (SMM) environments (fig. 1). Some important local-to-regional sources or delivery mechanisms of Hg to the eastern Pacific Ocean may have been related to weathering and soil denudation, wildfires, precipitation, and volcanic activity.

The middle to late Miocene was marked by a global-scale transition from  $C_3$ -dominated forests and savannahs to grasslands and the evolution of the  $C_4$  photosynthesis pathway in grasses (e.g., E. J. Edwards et al., 2010; Strömberg, 2011). The transition may have altered pedogenesis and resulted in fewer O-horizons, a large reservoir for mercury (e.g., Amos et al., 2014; Schuster et al., 2018; many others). The emergence of  $C_4$ -dominant terrestrial ecosystems did not play the dominant role on the Hg records presented in this study because the majority of the sediments that were studied predate this evolutionary event, although there may be some temporal overlap (e.g., E. J. Edwards et al., 2010; Hancock et al., 2019). Longer-term variation in soil pedogenesis, and therefore Hg biogeochemistry, related to the expansion of grasslands should be considered when interpreting marginal marine Hg records during the later Miocene. Also associated with the transition to grasslands on a global scale is an increase in wildfire intensity (e.g., Keeley & Rundel, 2005) and possibly weathering and erosion (Hay et al., 2002; Retallack, 2001).

Wildfires can lead to increased Hg deposition in a region via 1) increased atmospheric Hg concentrations directly from burning biomass and soils (e.g., Friedli et al., 2001, 2009; Homann et al., 2015; Obrist et al., 2008) and 2) an increase of weatherable surfaces following the fire (i.e., soil destabilization; e.g., Burke et al., 2010). In the late Permian-earliest Triassic and Early Jurassic, increased wildfires associated with a changing climate appear to have contributed to sedimentary Hg anomalies (e.g., Grasby et al., 2017; Them et al., 2019). Mercury may become enriched in burned soils as the efficiency of organic complexation with atmospherically derived Hg increases in charred organic matter (e.g., Burke et al., 2010). The weathering and erosion of rocks and soils in hinterlands—in tandem with increased wildfires—are viable mechanisms for increased fluxes of Hg to coastal environments. Therefore, high soil and rock weatherability paired with regional precipitation dynamics and/or fire activity in western North America during the Miocene may have increased Hg fluxes to the study areas.

Volcanism is another important process that delivers Hg to the ocean/atmosphere system (e.g., B. A. Edwards et al., 2021; Pirrone et al., 2010; Pyle & Mather, 2003; Selin, 2009), although the estimated range of modern fluxes is large (see fig. 1). Mercury concentration and Hg/TOC enrichments in the geologic record are often attributed to this process (see Grasby et al., 2019 and references therein). Two types of volcanoes active in western North America during the Miocene will be further discussed here. The Columbia River flood basalts (Washington, Oregon, Idaho, and Nevada) may have introduced significant quantities of Hg to Earth's surface, but its eruption history is constrained to a narrow time range contemporaneous with the onset of the MCO (~16.7–15.9 Ma; Kasbohm & Schoene, 2018), and thus it likely preceded the deposition of sediments studied here (e.g., Hancock et al., 2019). It is possible, however, that Hg-enriched sediments that accumulated on land during the eruptive phase of the Columbia River flood basalts were subsequently weathered later in the Miocene. Mercury-enriched materials may have initially been transported to oceanic regions north of the study area, but water mass advection in a north-south direction may have carried Hg-rich water to the study region. This is an unlikely source of Hg to the study locations as Hg concentrations in basalts are low (Coderre & Steinhórrsson, 1977). Accumulation of Hg in soils in basalt-rich regions, may, however, lead to an important localized source of Hg in marine environments during subsequent weathering and erosion of those soils (see B. A. Edwards et al., 2024). It is also important to note that if our Hg records of the MMF units were controlled by CRB volcanism, then they should have resulted in much higher Hg/TOC values (*sensu* Grasby et al., 2019).

Local to regional volcanism and hydrothermal activity may have been important sources of Hg to the study region (direct delivery by gases and fluids). In the Miocene, southwestern California experienced significant regional magmatism linked to subducting microplates, rotation of blocks, rifting, and decompression melting of mantle materials (e.g., Busby & Putirka, 2009; Weigand et al., 2002). These tectonic relationships resulted in several volcanic provinces that formed along the California coast (e.g., the Conejo Volcanics and Santa Maria Province, ca. 19–14 Ma; e.g., Stanley et al., 2000; Weigand et al., 2002 and references therein) as well as several events in the Sierra Nevada (Busby & Putirka, 2009). Beyond the direct input of Hg from these Middle Miocene basaltic and andesitic lavas, subsequent weathering of these igneous and metamorphic deposits may have also led to elevated Hg fluxes. The lower portions of each study site contain the largest sedimentary Hg enrichments and generally higher Hg/TOC and Hg/Al values, suggesting an increased flux of Hg to the basins. The ages of the basal studied MMF deposits may overlap with many of the southern California volcanic episodes (ca. 14 Ma) as evidenced by the presence of ash beds in each of the three locations, but particularly in SJB (e.g., Hancock et al., 2019; Weigand et al., 2002; and references therein). Furthermore, the elevated Hg values in the lower half of the SBB section correspond to the greater preservation of ash layers in this portion of stratigraphy (e.g., Homafius, 1994). It is cur-



rently unknown if the ash preservation in these basins is a product of the locally anoxic water column and sediments precluding heavy bioturbation or a feature of bottom-water current-induced erosion. Regardless, the proximity of these volcanic systems (e.g., Weigand et al., 2002) to the study area cannot be ignored.

Although the California volcanic suite might be seen as a candidate for the abundant volcanic ash and tephra beds in the MMF, recent work has instead linked these features with sources from the Snake River Plain in northern Nevada and eastern Idaho, along with volcanoes from southern Nevada (e.g., Knott et al., 2022). It is difficult to attribute our observed variability in Hg accumulation among the MMF sedimentary basins studied to such distant volcanic activity. Specifically, atmospheric fallout of Hg from distal volcanism should not have been differentially focused among basins that are in such close geographic proximity (e.g., San Joaquin Basin, Santa Barbara Basin, Santa Maria Basin).

The Sierra Nevada are associated with three tectonic events during the Miocene (~16 Ma, ~11–10 Ma, and ~8–7 Ma; Busby & Putirka, 2009). Considering the age of the MMF deposits studied here (see age model in Hancock et al., 2019), the second event (~11–10 Ma) is the only likely candidate to have contributed large amounts of Hg that could have been imprinted in these geochemical records. This event is associated with subduction-related explosive volcanism, which would have increased the flux of Hg to the study region (see B. A. Edwards et al., 2021). It is striking that none of the study sites displays elevated Hg/TOC values during this interval of intense regional volcanism. It is instead more likely that a combination of basin-specific factors led to the inter-site differences observed in our Hg chemostratigraphic profiles (see next section).

#### 7.4. Uniqueness of depositional conditions within the Miocene Monterey Formation

Although the elevated Hg concentrations in the MMF deposits may initially be interpreted as a result of elevated fluxes of Hg into the basins, it is also necessary to consider the local depositional environments. The MMF deposits contain elevated TOC contents and, when paired with local redox conditions in the basins (anoxic and often euxinic), likely led to an effective sink for the accumulation of RSEs (e.g., Hg, Mo, V, U; e.g., Hancock et al., 2019; Lau et al., 2022; see Tribovillard et al., 2006). The locally reducing conditions paired with enhanced bioproductivity and sulfide formation in a euxinic water column at certain intervals (e.g., Hancock et al., 2019; Lau et al., 2022) likely led to enhanced particle reactivity. This combination caused increased scavenging and a concomitant sequestration and burial of Hg into the sediments—although the exact mechanism of Hg cycling may have varied spatiotemporally in the study interval. Even though sediment accumulation rates likely varied during the study interval, they were generally low (e.g., Föllmi et al., 2005), which could have also favored elevated Hg concentrations. In modern environments, diatomaceous oozes have been suggested to represent an efficient sink of anthropogenic (and natural) sources of Hg in

the oceans (e.g., Zaferani et al., 2018). Although it is unclear whether the organic matter type (e.g., presence of diatomite and porcellanite indicative of siliceous organisms) in MMF deposits resulted in a greater export capacity, it must be considered. Overall, it is probable that the unique source-to-sink dynamics of the region played a role in the observed geochemical relationships.

The MMF deposits contain appreciable amounts of organic sulfur as previously discussed (e.g., Hancock et al., 2019; this study). Although the sulfurization of organic matter may have been important during ancient mass extinction events and other intervals of global environmental deterioration (e.g., Raven et al., 2018), it has not yet been considered whether organic sulfur compounds constitute a significant host of Hg across Earth history. In the SJB, Hg and organic sulfur are only weakly correlated ( $r^2 = 0.10$ ). In the SMB, Hg and organic sulfur are not correlated ( $r^2 = 0.02$ ). In the SBB, Hg and organic sulfur are moderately correlated ( $r^2 = 0.58$ ). Therefore, sulfurized organic matter could play a subordinate role in hosting Hg in sediments, but it must be assessed on a basin-to-basin basis. Organic sulfur compounds, however, take on additional importance because they may lead to overestimation of TS values—ultimately leading to inaccurate estimations of the role that sulfide played in local Hg cycling (figs. 6–8).

Although Hg concentrations in the MMF are generally higher than the Phanerozoic average, there are few significant Hg/TOC anomalies (figs. 3–5). This absence is likely driven by the significant TOC enrichments due to high productivity along with enhanced preservation under the predominantly anoxic and reducing conditions in the water column and sediments. Well over 99% of Phanerozoic Hg/TOC anomalies previously compiled occur in samples with extremely low TOC values ( $\ll 0.3\%$ ), thus obfuscating whether the identified anomalous intervals are driven by input fluxes of atmospherically derived Hg, output fluxes driven by changes in the local depositional environment, or even diagenesis or weathering that may affect Hg/TOC values (e.g., Charbonnier et al., 2020; Grasby et al., 2019; Park et al., 2022). This study serves as a foundation with broad relevance for tracking the importance of local controls, specifically varying behavior of Hg in redox environments that were generally reducing during an extended interval not associated with LIP volcanism. Because of suspected volcanic drivers, many intervals in geologic history associated with dramatic shifts in climate and biotic turnover have been targets for Hg analysis. These intervals, however, are also often characterized by global environmental deterioration to the point of widespread anoxia. Consequently, it is likely that local transitions to anoxic and reducing environments occurred and increased the efficiency in which Hg accumulated and was eventually preserved—independent of varying volcanic inputs. These relationships raise important cautionary flags demanding careful use of Hg as a proxy for volcanic inputs. Best practices might demand complementary Hg isotope analyses (Grasby et al., 2019) and certainly should include a full paleoenvironmental context for the chosen samples.

According to Grasby et al. (2015, 2019), enhanced Hg uptake into sediments through a volcanic source should be easily identifiable using log-log relationships (fig. 9). Geochemical data from the MMF deposits do not support the blanket use of these plots. First, it is thought that as Hg supersaturates a basin, that sediment uptake is transferred from organic matter to sulfide, therefore leading distinct locations in the log-log plot where the data will populate (Grasby et al., 2015, 2019). It is clear, however, that Hg uptake via sulfide formation and burial in the MMF deposits did not significantly alter the positioning of data points within these plots (fig. 9). Therefore, it is possible to have Hg uptake into sediments via sulfide without necessitating a large volcanic source of mercury. Second, the only two samples of the entire MMF dataset that surpass the threshold for “maximum normal drawdown” that would be expected to plot in the “sulfide drawdown” zone do not have elevated pyrite concentrations (fig. 7). If the sources of Hg in these two samples were from direct volcanic emissions or hydrothermal vents, then it is not apparent (fig. 9). Third, considering the proximity of the MMF deposits to active volcanic centers, the measured Hg concentrations should, in theory, be much higher and plot in the volcanic portion of the log-log plot. Hydrothermal fluids in marine settings contain high quantities of Hg (e.g., K. L. Bowman et al., 2015; Crepo-Medina et al., 2009; Lamborg et al., 2006), and the depositional setting of the MMF in a tectonically and volcanically active region of the eastern Pacific Ocean should have led to sedimentary Hg concentrations that are higher than observed. There may have been an elevated background of Hg input from these proximal volcanic sources (see Busby & Putirka, 2009; Weigand et al., 2002), but local depositional controls determined the intersite differences on uptake (partitioning) – suggesting that broad inputs and local controls on burial are a key combination in the observed geochemical profiles. Therefore, specific Hg or Hg/TOC spikes should be viewed cautiously in terms of volcanic inputs/events, but the overall enrichment with local overprints may represent a volcanic fingerprint in sediments. Other volcanically-derived elemental abundances and isotopic signatures should be paired with Hg data to rule out additional processes that can lead to observed enrichments.

### 7.5. Mercury poisoning in the Miocene oceans?

The sedimentary Hg values measured in this study represent some of the highest sustained concentrations known for the Phanerozoic (e.g., Grasby et al., 2019). This interval within the Miocene, however, is not typically associated with LIP emplacement or widespread biodiversity crises in marine or terrestrial locations. The end of the MCO and transition between the middle and late Miocene are associated with an extinction of ectothermic vertebrates in Europe, likely driven by changes in average temperatures, but this event appears to have been regional (e.g., Böhme, 2003). Studies have suggested that increased Hg loading in surface environments contributed to multiple mass extinction events through Hg poisoning (e.g., Bond & Grasby, 2017; Grasby et al., 2020; Lindström et al., 2019; Rakociński

et al., 2020). If this mechanism contributed to large-scale extinctions throughout the Phanerozoic, then a simple question results from this work, “Why are there no widespread ill-effects during the multi-million-year interval of highly elevated Hg concentrations described in this study?” The likely explanation is that the large magnitude of Hg loading observed in this study was more likely the result of local depositional environments, and therefore should not be expected to be relevant on a global scale (e.g., Them et al., 2019). We stress that the Hg data from the MMF cannot be assumed to be similar to other portions of the global ocean or even other proximal locations in the Pacific Ocean. Studies of other Miocene sedimentary deposits will be necessary to test for the regional extent of synchronous MMF-like Hg enrichments. Our data argue that increased Hg concentrations in a given region cannot *a priori* be ascribed as a driver of extinction, unless the full regional/global extent of enrichment is known. It is also difficult to distinguish between the cause of elevated Hg accumulation in any given basin unless multiproxy geochemical datasets are generated that can rule out other pathways. Our new data, for example, suggest that elevated burial efficiency of Hg, rather than elevated sources of Hg to a basin, can also be responsible for high sedimentary Hg concentrations that may be incorrectly used to argue for increased toxicities of ancient oceans as a driver of large-scale extinctions (e.g., Bond & Grasby, 2017). In other words, the range of sedimentary Hg concentrations may not reflect the atmospheric or marine reservoirs of mercury, but instead, may be associated with burial efficiency in a given environment.

### 7.6. Mercury burial in the Monterey Formation

To compare the amount of Hg sequestered in the MMF in these basins to global shelf environments, we first estimated the volume of Monterey rock in the basins via published or industry isopach maps. For the Santa Barbara-Ventura Basin (Naples Beach section), we calculated a modern volume of 3770 km<sup>3</sup>. Using a bulk density of 1.9 g/cm<sup>3</sup>, there are ~7.2 × 10<sup>18</sup> g of sediment in this basin. Using the average Hg concentration from Naples Beach (89.45 ng/g) yields ~6.4 × 10<sup>5</sup> Mg of Hg. If we estimate that deposition occurred over 11 million years (Barron, 2022), then this constitutes 0.06 Mg of Hg per year.

For the San Joaquin Basin (Thorndyke drill core, including Antelope and McDonald Shale members), we calculated a modern volume of 4600 km<sup>3</sup>. Using a bulk density of 1.9 g/cm<sup>3</sup>, there are >8.7 × 10<sup>18</sup> g of sediment in this basin. Using the average Hg concentration from Thorndyke (98.29 ng/g) results in an estimate of ~8.6 × 10<sup>5</sup> Mg of Hg. If we consider that deposition occurred over 7 million years (Hosford-Scheirer & Magoon, 2008), then this constitutes 0.12 Mg of Hg per year.

For the Santa Maria Basin (Union Leroy drill core), we calculated a modern volume of 1900 km<sup>3</sup> for the MMF. Using the same bulk density of 1.9 g/cm<sup>3</sup>, there are ~3.6 × 10<sup>18</sup> g of sediment in this basin. Using the average Hg concentration from Thorndyke (311.64 ng/g) results in ~11.3 × 10<sup>5</sup> Mg of Hg. If we estimate that deposition occurred over 10.2

million years (Isaacs, 2001; White et al., 1992), the result is 0.11 Mg of Hg per year.

It is important to note that there has been significant uplift and erosion in all of these basins, so these calculations represent minimum values and are likely much higher. Furthermore, the volume and time-span analyzed for the San Joaquin basin (Antelope and McDonald members) represent only the major portion of the MMF, but it does not include the older/lower portion, which has been historically difficult to measure and correlate. While noting these caveats, we then compared Hg deposition from these basins (total of 0.29 Mg/a) to estimates of global and continental shelf Hg deposition. Approximately 200 Mg Hg is deposited in marine sediments each year in the modern world (see Schuster et al., 2018). If continental shelves represent ~10% of the total ocean area, assuming that the same amount of Hg is buried in shelf environments as the rest of the ocean, then ~20 Mg of Hg is currently buried on shelves each year. Therefore, burial of Hg in the studied MMF deposits represents about 1.5% of the total Hg buried in modern continental shelf environments.

Notably, these three basins cover ~27,000 km<sup>3</sup>, which is ~1/1000<sup>th</sup> of the total shelfal area of the modern global ocean. Thus, the mass accumulation rates (MARs, defined as accumulation/area/time) in these basins are ~10x greater than the modern shelfal average. This enhanced burial is likely due to a combination of many proximal factors that led to such high accumulation rates of Hg and likely many other elements and minerals. The combination of neotectonism and active volcanism in the hinterland may have led to an increased flux of continental-derived materials that filled these semi-enclosed basins, adsorbing Hg onto the particles during transport. The local redox conditions in these basins (dysoxic to sulfidic) also led to enhanced accumulation of pyrite and other reduced minerals, which would have scavenged Hg, as discussed above. Last, these highly productive environments would have also sequestered a significant amount of Hg in association with organic matter, as discussed above. Overall, the true value for proportion of total Hg burial during the Miocene in the MMF is likely significantly higher due to the high calculated MARs paired with the predicted amounts of uplift and erosion that have substantially reduced the estimates. Keeping this in mind, our studied basins also represent only a portion of the total extent of the Miocene Monterey Formation. As such, the entirety of the MMF likely represented a major sink of Hg during the Miocene.

### 7.7. Outlook

This research was focused on the biogeochemical cycling of Hg in OM-rich, pyritic shales deposited under predominantly reducing conditions during a non-LIP interval (e.g., Hancock et al., 2019) to remove the impact that LIP-derived Hg would have on sedimentary Hg accumulation (Grasby et al., 2019). It remains unclear, therefore, what role redox plays in OM-lean sediments that may have been deposited under oxic or vacillating redox conditions, but it is likely that the Hg cycle would be affected (Frieling et al., 2023). Extrapolating our conclusions for the MMF deposits, we

posit that the microbial cycling of sulfur and production of sulfide coupled with iron reduction in these types of environments likely impacted the Hg cycle across ancient climatic events. This possibility can be tested through multiproxy datasets that include direct measures of pyrite content. Mercury can also be associated with multiple host phases (e.g., organic matter, pyrite, clay minerals) in organic-rich sediments as observed in the MMF deposits, suggesting that the degree of organic matter richness does not preclude any given host phase from being dominant over another. As our efforts continue to determine the links between ancient large-scale volcanism and environmental and biological evolution, the role of redox variability must be constrained before interpretations can be made. This is especially important for redox-sensitive elements such as mercury, molybdenum, and tellurium, which all are intimately associated with the cycling of sulfur in the water column and sediments.

## 8. CONCLUSIONS

Three basins from the eastern Pacific Ocean containing the Miocene Monterey Formation were studied to elucidate the role of varying environmental parameters that may influence the transportation, accumulation, and preservation of mercury in sediments in reducing environments. In each basin, Hg deposition was controlled by either redox (e.g., sulfide preservation), detrital input via clay minerals, organic matter loading, and/or a combination of the three. Significantly, each basin is associated with different dominant host phases for Hg, thus providing new insights into the complexity of Hg cycling even at locations geographically close to one another that display minor variation in redox conditions over 10<sup>6</sup>-yr timescales. It is presently unclear whether changes in source fluxes of Hg led to the observed Hg enrichments in the study interval, but application of Hg isotopes on these sediments may help unmix some of these processes. It is clear, however, that the locally reducing conditions in the basins enhanced Hg accumulation. The MMF multiproxy datasets also suggest many of the common proxies (e.g., TS, FeT, and Mo concentrations) used to estimate pyrite concentrations may yield unreliable interpretations. We recommend that pyrite concentrations be determined directly in studies of Hg enrichment to help rule out the role of local redox. Ancient intervals of widespread environmental deterioration are often associated with the deposition of OM-rich sediments, so elucidating the controls on metal deposition requires diverse data types, such as those presented in this study. Considering the complexity we observed from locations with subtle variations in local redox, we can surmise that interpretations of Hg cycling at other locations with fluctuating redox on comparatively short timescales would also require thorough assessment of the processes that may have led to Hg enrichment. Nonetheless, the proximity to local volcanoes may not lead to the large Hg/TOC enrichments often expected given the large Hg fluxes from these systems. Considering this, we suggest that at least some of the large sedimentary Hg/TOC enrichments observed in the past can be

related to the enhanced mobilization of Hg due to biogeochemical feedbacks associated with phenomena that can perturb the Earth system (e.g., massive volcanoes, impacts, etc.) rather than direct volcanogenic outgassing of mercury. Only when Hg data are measured in tandem with other geochemical data to rule out volcanism as the sole cause of Hg enrichment will it be possible to more accurately use sedimentary Hg geochemistry to reconstruct the temporal evolution of some intervals of large-scale magmatism. It is also ideal to study different locations of the same age with different environmental conditions.

.....

#### ACKNOWLEDGMENTS

TRT would like to thank the College of Charleston for startup funds that contributed to this project. The Petroleum Research Fund of the American Chemical Society and the NASA Interdisciplinary Consortia for Astrobiology Research (ICAR) Program provided funds to TWL. We would like to thank Aera Energy, LLC for providing access to sam-

ples and data from the Thorndyke core. The authors who like to thank Judith Hannah and Bradley Sageman for constructive criticisms that ultimately improved this manuscript.

#### AUTHOR CONTRIBUTIONS

T.R.T. designed the study. L.G.H. and R.J.B. collected the samples. T.R.T., C.L.M., and M.D.K. conducted the Hg analyses. C.J.T. conducted the pyrite and T.S. analyses under the supervision of T.W.L. T.R.T. wrote the paper with contributions from all the authors. T.R.T. prepared the figures.

#### DATA AVAILABILITY STATEMENT

The data can be found in the supplemental information: <https://doi.org/10.17605/OSF.IO/NWQRY>

Editor: C. Page Chamberlain, Associate Editor: Brad Sageman

Submitted: August 04, 2023 EST, Accepted: July 29, 2024 EST



This is an open-access article distributed under the terms of the Creative Commons Attribution 4.0 International License (CCBY-4.0). View this license's legal deed at <http://creativecommons.org/licenses/by/4.0> and legal code at <http://creativecommons.org/licenses/by/4.0/legalcode> for more information.



## REFERENCES

- Algeo, T. J. (2004). Can marine anoxic events draw down the trace element inventory of seawater? *Geology*, 32(12), 1057. <https://doi.org/10.1130/g20896.1>
- Algeo, T. J., & Lyons, T. W. (2006). Mo-total organic carbon covariation in modern anoxic marine environments: Implications for analysis of paleoredox and paleohydrographic conditions. *Paleoceanography*, 21(1). <https://doi.org/10.1029/2004pa001112>
- Amos, H. M., Jacob, D. J., Kocman, D., Horowitz, H. M., Zhang, Y., Dutkiewicz, S., Horvat, M., Corbitt, E. S., Krabbenhoft, D. P., & Sunderland, E. M. (2014). Global Biogeochemical Implications of Mercury Discharges from Rivers and Sediment Burial. *Environmental Science & Technology*, 48(16), 9514–9522. <https://doi.org/10.1021/es502134t>
- Barnette, C. (2015). *Re-Os Geochronology of the Monterey Formation, Union Leroy 51-18 Well, Santa Maria Basin, California* [M.S. thesis, University of Houston]. <http://hdl.handle.net/10657/1944>
- Barron, J. A. (1986). Paleocyanographic and tectonic controls on deposition of the Monterey Formation and related siliceous rocks in California. *Palaeogeography, Palaeoclimatology, Palaeoecology*, 53(1), 27–45. [https://doi.org/10.1016/0031-0182\(86\)90037-4](https://doi.org/10.1016/0031-0182(86)90037-4)
- Barron, J. A. (2022). Refined assessment of the paleocyanographic and tectonic influences on the deposition of the Monterey Formation in California. In *Understanding the Monterey Formation and Similar Biosiliceous Units across Space and Time* (pp. 113–127). [https://doi.org/10.1130/2022.2556\(06\)](https://doi.org/10.1130/2022.2556(06))
- Barron, J. A., & Isaacs, C. M. (2001). Updated Chronostratigraphic framework for the California Miocene. In C. M. Isaacs & J. Rullkötter (Eds.), *The Monterey Formation: From Rocks to Molecules* (pp. 393–395). Columbia Univ. Press.
- Barry, T. L., Kelley, S. P., Reidel, S. P., Camp, V. E., Self, S., Jarboe, N. A., Duncan, R. A., & Renne, P. R. (2013). Eruption chronology of the Columbia River Basalt Group. *The Columbia River Flood Basalt Province*. [https://doi.org/10.1130/2013.2497\(02\)](https://doi.org/10.1130/2013.2497(02))
- Batrakova, N., Travnikov, O., & Rozovskaya, O. (2014). Chemical and physical transformations of mercury in the ocean: a review. *Ocean Science*, 10(6), 1047–1063. <https://doi.org/10.5194/os-10-1047-2014>
- Behl, R. J. (1999). Since Bramlette (1946): the Miocene Monterey Formation of California revisited. *Classic Cordilleran Concepts: A View from California*. <https://doi.org/10.1130/0-8137-2338-8.301>
- Berner, R. A. (1984). Sedimentary pyrite formation: An update. *Geochimica et Cosmochimica Acta*, 48(4), 605–615. [https://doi.org/10.1016/0016-7037\(84\)90089-9](https://doi.org/10.1016/0016-7037(84)90089-9)
- Bessinger, B. A. (2014). Use of Stable Isotopes to Identify Sources of Mercury in Sediments: A Review and Uncertainty Analysis. *Environmental Forensics*, 15(3), 265–280. <https://doi.org/10.1080/15275922.2014.930939>
- Blakey, R. (2014). *Colorado Plateau Geosystems, Inc.: Reconstructing the Ancient EARTH*. <https://deeptimemaps.com>
- Blum, J. D., Sherman, L. S., & Johnson, M. W. (2014). Mercury Isotopes in Earth and Environmental Sciences. *Annual Review of Earth and Planetary Sciences*, 42(1), 249–269. <https://doi.org/10.1146/annurev-earth-050212-124107>
- Böhme, M. (2003). The Miocene Climatic Optimum: evidence from ectothermic vertebrates of Central Europe. *Palaeogeography, Palaeoclimatology, Palaeoecology*, 195(3–4), 389–401. [https://doi.org/10.1016/s0031-0182\(03\)00367-5](https://doi.org/10.1016/s0031-0182(03)00367-5)
- Bond, D. P. G., & Grasby, S. E. (2017). On the causes of mass extinctions. *Palaeogeography, Palaeoclimatology, Palaeoecology*, 478, 3–29. <https://doi.org/10.1016/j.palaeo.2016.11.005>
- Bower, J., Savage, K. S., Weinman, B., Barnett, M. O., Hamilton, W. P., & Harper, W. F. (2008). Immobilization of mercury by pyrite (FeS<sub>2</sub>). *Environmental Pollution*, 156(2), 504–514. <https://doi.org/10.1016/j.envpol.2008.01.011>
- Bowman, C. N., Them, T. R., II, Knight, M. D., Kaljo, D., Eriksson, M. E., Hints, O., Martma, T., Owens, J. D., & Young, S. A. (2021). A multi-proxy approach to constrain reducing conditions in the Baltic Basin during the late Silurian Lau carbon isotope excursion. *Palaeogeography, Palaeoclimatology, Palaeoecology*, 581, 110624. <https://doi.org/10.1016/j.palaeo.2021.110624>
- Bowman, K. L., Hammerschmidt, C. R., Lamborg, C. H., & Swarr, G. (2015). Mercury in the North Atlantic Ocean: The U.S. GEOTRACES zonal and meridional sections. *Deep Sea Research Part II: Topical Studies in Oceanography*, 116, 251–261. <https://doi.org/10.1016/j.dsr2.2014.07.004>

- Bramlette, M. N. (1946). *The Monterey Formation of California and the origin of its siliceous rocks*. US Government Printing Office. <https://doi.org/10.3133/pp21>
- Burke, M. P., Hogue, T. S., Ferreira, M., Mendez, C. B., Navarro, B., Lopez, S., & Jay, J. A. (2010). The Effect of Wildfire on Soil Mercury Concentrations in Southern California Watersheds. *Water, Air, & Soil Pollution*, 212(1–4), 369–385. <https://doi.org/10.1007/s11270-010-0351-y>
- Busby, C. J., & Putirka, K. (2009). Miocene evolution of the western edge of the Nevadaplano in the central and northern Sierra Nevada: palaeocanyons, magmatism, and structure. *International Geology Review*, 51(7–8), 670–701. <https://doi.org/10.1080/00206810902978265>
- Canfield, D. E., Raiswell, R., Westrich, J. T., Reaves, C. M., & Berner, R. A. (1986). The use of chromium reduction in the analysis of reduced inorganic sulfur in sediments and shales. *Chemical Geology*, 54(1–2), 149–155. [https://doi.org/10.1016/0009-2541\(86\)90078-1](https://doi.org/10.1016/0009-2541(86)90078-1)
- Chappaz, A., Lyons, T. W., Gregory, D. D., Reinhard, C. T., Gill, B. C., Li, C., & Large, R. R. (2014). Does pyrite act as an important host for molybdenum in modern and ancient euxinic sediments? *Geochimica et Cosmochimica Acta*, 126, 112–122. <https://doi.org/10.1016/j.gca.2013.10.028>
- Charbonnier, G., Adatte, T., Föllmi, K. B., & Suan, G. (2020). Effect of Intense Weathering and Postdepositional Degradation of Organic Matter on Hg/TOC Proxy in Organic-rich Sediments and its Implications for Deep-Time Investigations. *Geochemistry, Geophysics, Geosystems*, 21(2). <https://doi.org/10.1029/2019gc008707>
- Chen, D., Ren, D., Deng, C., Tian, Z., & Yin, R. (2022). Mercury loss and isotope fractionation during high-pressure and high-temperature processing of sediments: Implication for the behaviors of mercury during metamorphism. *Geochimica et Cosmochimica Acta*, 334, 231–240. <https://doi.org/10.1016/j.gca.2022.08.010>
- Chen, J., Sun, G., Lu, B., Ma, R.-Y., Xiao, Z., Cai, Y.-F., Zhang, H., Shen, S.-Z., Zhang, F., & Feng, Z. (2023). Inconsistent mercury records from terrestrial upland to coastal lowland across the Permian-Triassic transition. *Earth and Planetary Science Letters*, 614, 118195. <https://doi.org/10.1016/j.epsl.2023.118195>
- Coderre, J. A., & Steinthórsson, S. (1977). Natural concentrations of mercury in Iceland. *Geochimica et Cosmochimica Acta*, 41(3), 419–424. [https://doi.org/10.1016/0016-7037\(77\)90270-8](https://doi.org/10.1016/0016-7037(77)90270-8)
- Crepeo-Medina, M., Chatziefthimiou, A. D., Bloom, N. S., Luther, G. W. I., Wright, D. D., Reinfelder, J. R., Vetricani, C., & Barkay, T. (2009). Adaptation of chemosynthetic microorganisms to elevated mercury concentrations in deep-sea hydrothermal vents. *Limnology and Oceanography*, 54(1), 41–49. <https://doi.org/10.4319/lo.2009.54.1.0041>
- Curiale, J. A., & Odermatt, J. R. (1989). Short-term biomarker variability in the Monterey formation, Santa Maria Basin. *Organic Geochemistry*, 14(1), 1–13. [https://doi.org/10.1016/0146-6380\(89\)90014-4](https://doi.org/10.1016/0146-6380(89)90014-4)
- Das, R., Bizimis, M., & Wilson, A. M. (2013). Tracing mercury seawater vs. atmospheric inputs in a pristine SE USA salt marsh system: Mercury isotope evidence. *Chemical Geology*, 336, 50–61. <https://doi.org/10.1016/j.chemgeo.2012.04.035>
- Driscoll, C. T., Mason, R. P., Chan, H. M., Jacob, D. J., & Pirrone, N. (2013). Mercury as a Global Pollutant: Sources, Pathways, and Effects. *Environmental Science & Technology*, 47(10), 4967–4983. <https://doi.org/10.1021/es305071v>
- Duan, Y., Han, D. S., Batchelor, B., & Abdel-Wahab, A. (2016). Synthesis, characterization, and application of pyrite for removal of mercury. *Colloids and Surfaces A: Physicochemical and Engineering Aspects*, 490, 326–335. <https://doi.org/10.1016/j.colsurfa.2015.11.057>
- Edwards, B. A., Kushner, D. S., Outridge, P. M., & Wang, F. (2021). Fifty years of volcanic mercury emission research: Knowledge gaps and future directions. *Science of The Total Environment*, 757, 143800. <https://doi.org/10.1016/j.scitotenv.2020.143800>
- Edwards, B. A., Outridge, P. M., & Wang, F. (2024). Mercury from Icelandic geothermal activity: High enrichments in soils, low emissions to the atmosphere. *Geochimica et Cosmochimica Acta*, 378, 286–299. <https://doi.org/10.1016/j.gca.2024.06.026>
- Edwards, E. J., Osborne, C. P., Strömberg, C. A. E., Smith, S. A., C4 Grasses Consortium, Bond, W. J., Christin, P.-A., Cousins, A. B., Duvall, M. R., Fox, D. L., Freckleton, R. P., Ghannoum, O., Hartwell, J., Huang, Y., Janis, C. M., Keeley, J. E., Kellogg, E. A., Knapp, A. K., Leakey, A. D. B., & Tipler, B. (2010). The Origins of C4 Grasslands: Integrating Evolutionary and Ecosystem Science. *Science*, 328(5978), 587–591. <https://doi.org/10.1126/science.1177216>
- Erickson, B. E., & Helz, G. R. (2000). Molybdenum(VI) speciation in sulfidic waters: *Geochimica et Cosmochimica Acta*, 64(7), 1149–1158. [https://doi.org/10.1016/s0016-7037\(99\)00423-8](https://doi.org/10.1016/s0016-7037(99)00423-8)

- Fendley, I. M., Frieling, J., Mather, T. A., Ruhl, M., Hesselbo, S. P., & Jenkyns, H. C. (2024). Early Jurassic large igneous province carbon emissions constrained by sedimentary mercury. *Nature Geoscience*, 17(3), 241–248. <https://doi.org/10.1038/s41561-024-01378-5>
- Fitzgerald, W. F., & Lamborg, C. H. (2014). Geochemistry of Mercury in the Environment. *Treatise on Geochemistry*, 91–129. <https://doi.org/10.1016/b978-0-08-095975-7.00904-9>
- Flower, B. P., & Kennett, J. P. (1994). The middle Miocene climatic transition: East Antarctic ice sheet development, deep ocean circulation and global carbon cycling. *Palaeogeography, Palaeoclimatology, Palaeoecology*, 108(3–4), 537–555. [https://doi.org/10.1016/0031-0182\(94\)90251-8](https://doi.org/10.1016/0031-0182(94)90251-8)
- Föllmi, K. B., Badertscher, C., de Kaenel, E., Stille, P., John, C. M., Adatte, T., & Steinmann, P. (2005). Phosphogenesis and organic-carbon preservation in the Miocene Monterey Formation at Naples Beach, California—the Monterey hypothesis revisited. *GSA Bulletin*, 117, 589–619. <https://doi.org/10.1130/B25524.1>
- Föllmi, K. B., Thomet, P., Lévy, S., De Kaenel, E., Spangenberg, J. E., Adatte, T., Behl, R. J., & Garrison, R. E. (2017). The Impact of Hydrodynamics, Authigenesis, and Basin Morphology On Sediment Accumulation In An Upwelling Environment: The Miocene Monterey Formation At Shell Beach and Mussel Rock (Pismo and Santa Maria Basins, Central California, U.S.A.). *Journal of Sedimentary Research*, 87(9), 986–1018. <https://doi.org/10.2110/jsr.2017.57>
- Friedli, H. R., Arellano, A. F., Cinnirella, S., & Pirrone, N. (2009). Initial estimates of mercury emissions to the atmosphere from global biomass burning. *Environmental Science & Technology*, 43(10), 3507–3513. <https://doi.org/10.1021/es802703g>
- Friedli, H. R., Radke, L. F., & Lu, J. Y. (2001). Mercury in smoke from biomass fires. *Geophysical Research Letters*, 28(17), 3223–3226. <https://doi.org/10.1029/2000gl012704>
- Frieling, J., Mather, T. A., März, C., Jenkyns, H. C., Hennekam, R., Reichart, G. J., Slomp, C. P., & van Helmond, N. A. G. M. (2023). Effects of redox variability and early diagenesis on marine sedimentary Hg records. *Geochimica et Cosmochimica Acta*, 351, 78–95. <https://doi.org/10.1016/j.gca.2023.04.015>
- Garrison, R. E., & Graham, S. A. (1984). Early diagenetic dolomites and the origin of dolomite-bearing breccias, lower Monterey Formation, Arroyo Seco, Monterey County, California. In R. E. Garrison, M. Kastner, & D. H. Zenger (Eds.), *Dolomites of The Monterey Formation and Other Organic-Rich Units 41* (pp. 87–101). Pacific Section SEPM.
- Graham, S. A., & Williams, L. A. (1985). Tectonic, depositional, and diagenetic history of the Monterey Formation (Miocene), central San Joaquin basin, California. *AAPG Bulletin*, 69, 385–411. <https://doi.org/10.1306/ad4624f7-16f7-11d7-8645000102c1865d>
- Grasby, S. E., Beauchamp, B., Bond, D. P. G., Wignall, P., Talavera, C., Galloway, J. M., Piepjohn, K., Reinhardt, L., & Blomeier, D. (2015). Progressive environmental deterioration in northwestern Pangea leading to the latest Permian extinction. *GSA Bulletin*, 127(9–10), 1331–1347. <https://doi.org/10.1130/b31197.1>
- Grasby, S. E., Liu, X., Yin, R., Ernst, R. E., & Chen, Z. (2020). Toxic mercury pulses into late Permian terrestrial and marine environments. *Geology*, 48(8), 830–833. <https://doi.org/10.1130/g47295.1>
- Grasby, S. E., Sanei, H., Beauchamp, B., & Chen, Z. (2013). Mercury deposition through the Permo–Triassic Biotic Crisis. *Chemical Geology*, 351, 209–216. <https://doi.org/10.1016/j.chemgeo.2013.05.022>
- Grasby, S. E., Shen, W., Yin, R., Gleason, J. D., Blum, J. D., Lepak, R. F., Hurley, J. P., & Beauchamp, B. (2017). Isotopic signatures of mercury contamination in latest Permian oceans. *Geology*, 45(1), 55–58. <https://doi.org/10.1130/g38487.1>
- Grasby, S. E., Them, T. R., II, Chen, Z., Yin, R., & Ardakani, O. H. (2019). Mercury as a proxy for volcanic emissions in the geologic record. *Earth-Science Reviews*, 196, 102880. <https://doi.org/10.1016/j.earscirev.2019.102880>
- Gregory, D. D., Large, R. R., Halpin, J. A., Baturina, E. L., Lyons, T. W., Wu, S., Danyushevsky, L., Sack, P. J., Chappaz, A., Maslennikov, V. V., & Bull, S. W. (2015). Trace Element Content of Sedimentary Pyrite in Black Shales. *Economic Geology*, 110(6), 1389–1410. <https://doi.org/10.2113/econgeo.110.6.1389>
- Gu, X., Heaney, P. J., Reis, F. D. A. A., & Brantley, S. L. (2020). Deep abiotic weathering of pyrite. *Science*, 370(6515). <https://doi.org/10.1126/science.abb8092>

- Hagen, A. P. I., Jones, D. S., Tosca, N. J., Fike, D. A., & Pruss, S. B. (2022). Sedimentary mercury as a proxy for redox oscillations during the Cambrian SPICE event in western Newfoundland. *Canadian Journal of Earth Sciences*, 59(8), 504–520. <https://doi.org/10.1139/cjes-2021-0108>
- Hancock, L. G., Hardisty, D. S., Behl, R. J., & Lyons, T. W. (2019). A multi-basin redox reconstruction for the Miocene Monterey Formation, California, USA. *Palaeogeography, Palaeoclimatology, Palaeoecology*, 520, 114–127. <https://doi.org/10.1016/j.palaeo.2019.01.031>
- Hardisty, D. S., Lyons, T. W., Riedinger, N., Isson, T. T., Owens, J. D., Aller, R. C., Rye, D. M., Planavsky, N. J., Reinhard, C. T., Gill, B. C., Masterson, A. L., Asael, D., & Johnston, D. T. (2018). An evaluation of sedimentary molybdenum and iron as proxies for pore fluid paleoredox conditions. *American Journal of Science*, 318(5), 527–556. <https://doi.org/10.2475/05.2018.04>
- Hay, W. W., Soeding, E., DeConto, R. M., & Wold, C. N. (2002). The late Cenozoic uplift–Climate change paradox. *International Journal of Earth Sciences*, 91(5), 746–774. <https://doi.org/10.1007/s00551-002-0263-1>
- Hedges, J. I., & Keil, R. G. (1995). Sedimentary organic matter preservation: an assessment and speculative synthesis. *Marine Chemistry*, 49(2–3), 81–115. [https://doi.org/10.1016/0304-4203\(95\)00008-f](https://doi.org/10.1016/0304-4203(95)00008-f)
- Herold, N., Huber, M., Müller, R. D., & Seton, M. (2012). Modeling the Miocene climatic optimum: Ocean circulation. *Paleoceanography*, 27(1). <https://doi.org/10.1029/2010pa002041>
- Holbourn, A., Kuhnt, W., Clemens, S., Prell, W., & Andersen, N. (2013). Middle to late Miocene stepwise climate cooling: Evidence from a high-resolution deep water isotope curve spanning 8 million years: MIOCENE BENTHIC ISOTOPES. *Paleoceanography*, 28(4), 688–699. <https://doi.org/10.1002/2013pa002538>
- Holbourn, A., Kuhnt, W., Kochhann, K. G. D., Andersen, N., & Sebastian Meier, K. J. (2015). Global perturbation of the carbon cycle at the onset of the Miocene Climatic Optimum. *Geology*, 43(2), 123–126. <https://doi.org/10.1130/g36317.1>
- Holmes, C. D., Jacob, D. J., Corbitt, E. S., Mao, J., Yang, X., Talbot, R., & Slemr, F. (2010). Global atmospheric model for mercury including oxidation by bromine atoms. *Atmospheric Chemistry and Physics*, 10(24), 12037–12057. <https://doi.org/10.5194/acp-10-12037-2010>
- Homafius, J. S. (1994). Correlation of volcanic ashes in the Monterey Formation between Naples Beach and Gaviota Beach, California. In *Field Guide to the Monterey Formation between Santa Barbara and Gaviota, California*. <https://doi.org/10.32375/1994-gb72.4>
- Homann, P. S., Darbyshire, R. L., Bormann, B. T., & Morrisette, B. A. (2015). Forest Structure Affects Soil Mercury Losses in the Presence and Absence of Wildfire. *Environmental Science & Technology*, 49(21), 12714–12722. <https://doi.org/10.1021/acs.est.5b03355>
- Hosford-Scheirer, A., & Magoon, L. B. (2008). Age, Distribution, and Stratigraphic Relationship of Rock Units in the San Joaquin Basin Province, California. *USGS Professional Paper*, 1733(05). <https://doi.org/10.3133/pp17135>
- Ingle, J. C., Jr. (1981). Origin of Neogene diatomites around the north Pacific rim. In R. E. Garrison & R. G. Douglas (Eds.), *The Monterey Formation and related siliceous rocks of California* (pp. 159–179). Pacific Section, Los Angeles SEPM.
- Isaacs, C. M. (2001). Depositional Framework of the Monterey Formation, California. In C. M. Isaacs & J. Rullkötter (Eds.), *The Monterey Formation: From Rocks to Molecules* (pp. 1–30). Columbia University Press.
- Isaacs, C. M., Pisciotto, K. A., & Garrison, R. E. (1983). Chapter 15 Facies and Diagenesis of the Miocene Monterey Formation, California: A Summary. *Developments in Sedimentology*, 247–282. [https://doi.org/10.1016/s0070-4571\(08\)70094-3](https://doi.org/10.1016/s0070-4571(08)70094-3)
- Jenkyns, H. C. (1988). The early Toarcian (Jurassic) anoxic event; stratigraphic, sedimentary and geochemical evidence. *American Journal of Science*, 288(2), 101–151. <https://doi.org/10.2475/ajs.288.2.101>
- Kalvoda, J., Kumpan, T., Qie, W., Frýda, J., & Bábek, O. (2019). Mercury spikes at the Devonian–Carboniferous boundary in the eastern part of the Rhenohercynian Zone (central Europe) and in the South China Block. *Palaeogeography, Palaeoclimatology, Palaeoecology*, 531, 109221. <https://doi.org/10.1016/j.palaeo.2019.05.043>
- Kasbohm, J., & Schoene, B. (2018). Rapid eruption of the Columbia River flood basalt and correlation with the mid-Miocene climate optimum. *Science Advances*, 4(9). <https://doi.org/10.1126/sciadv.aat8223>
- Katz, B. J., & Royle, R. A. (2001). Variability of Source Rock Attributes in the Monterey Formation, California. In C. M. Isaacs & J. Rullkötter (Eds.), *The Monterey Formation: From Rocks to Molecules* (pp. 107–130). Columbia University Press.



- Keeley, J. E., & Rundel, P. W. (2005). Fire and the Miocene expansion of C4 grasslands. *Ecology Letters*, 8(7), 683–690. <https://doi.org/10.1111/j.1461-0248.2005.00767.x>
- Keil, R. G., Tsamakis, E., Fuh, C. B., Giddings, J. C., & Hedges, J. I. (1994). Mineralogical and textural controls on the organic composition of coastal marine sediments: Hydrodynamic separation using SPLITT-fractionation. *Geochimica et Cosmochimica Acta*, 58(2), 879–893. [https://doi.org/10.1016/0016-7037\(94\)90512-6](https://doi.org/10.1016/0016-7037(94)90512-6)
- Kennedy, M. J., Pevear, D. R., & Hill, R. J. (2002). Mineral Surface Control of Organic Carbon in Black Shale. *Science*, 295(5555), 657–660. <https://doi.org/10.1126/science.1066611>
- Kennett, J. P. (1977). Cenozoic evolution of Antarctic glaciation, the circum-Antarctic Ocean, and their impact on global paleoceanography. *Journal of Geophysical Research*, 82(27), 3843–3860. <https://doi.org/10.1029/jc082i027p03843>
- Kim, J., Lim, D., Jeong, D., Xu, Z., Kim, H., Kim, J., & Kim, D. (2022). Mercury (Hg) geochemistry of mid-ocean ridge sediments on the Central Indian Ridge: Chemical forms and isotopic composition. *Chemical Geology*, 604, 120942. <https://doi.org/10.1016/j.chemgeo.2022.120942>
- Knott, J. R., Sarna-Wojcicki, A. M., Barron, J. A., Wan, E., Heizler, L., & Martinez, P. (2022). Tephrochronology of the Miocene Monterey and Modelo Formations, California. In *Understanding the Monterey Formation and Similar Biosiliceous Units across Space and Time* (pp. 187–214). [https://doi.org/10.1130/2022.2556\(08\)](https://doi.org/10.1130/2022.2556(08))
- Kongchum, M., Hudnall, W. H., & Delaune, R. D. (2011). Relationship between sediment clay minerals and total mercury. *Journal of Environmental Science and Health, Part A*, 46(5), 534–539. <https://doi.org/10.1080/10934529.2011.551745>
- Kovács, E. B., Ruhl, M., Demény, A., Fórizs, I., Hegyi, I., Horváth-Kostka, Z. R., Móricz, F., Vallner, Z., & Pálffy, J. (2020). Mercury anomalies and carbon isotope excursions in the western Tethyan Csővár section support the link between CAMP volcanism and the end-Triassic extinction. *Global and Planetary Change*, 194, 103291. <https://doi.org/10.1016/j.gloplacha.2020.103291>
- Lamborg, C. H., Von Damm, K. L., Fitzgerald, W. F., Hammerschmidt, C. R., & Zierenberg, R. (2006). Mercury and monomethylmercury in fluids from Sea Cliff submarine hydrothermal field, Gorda Ridge. *Geophysical Research Letters*, 33(17). <https://doi.org/10.1029/2006gl026321>
- Large, R. R., Halpin, J. A., Danyushevsky, L. V., Maslennikov, V. V., Bull, S. W., Long, J. A., Gregory, D. D., Lounejeva, E., Lyons, T. W., Sack, P. J., McGoldrick, P. J., & Calver, C. R. (2014). Trace element content of sedimentary pyrite as a new proxy for deep-time ocean-atmosphere evolution. *Earth and Planetary Science Letters*, 389, 209–220. <https://doi.org/10.1016/j.epsl.2013.12.020>
- Lau, K. V., Hancock, L. G., Severmann, S., Kuzminov, A., Cole, D. B., Behl, R. J., Planavsky, N. J., & Lyons, T. W. (2022). Variable local basin hydrography and productivity control the uranium isotope paleoredox proxy in anoxic black shales. *Geochimica et Cosmochimica Acta*, 317, 433–456. <https://doi.org/10.1016/j.gca.2021.10.011>
- Lavoie, R. A., Amyot, M., & Lapierre, J.-F. (2019). Global Meta-Analysis on the Relationship Between Mercury and Dissolved Organic Carbon in Freshwater Environments. *Journal of Geophysical Research: Biogeosciences*, 124(6), 1508–1523. <https://doi.org/10.1029/2018jg004896>
- Lindström, S., Sanei, H., van de Schootbrugge, B., Pedersen, G. K., Leshner, C. E., Tegner, C., Heunisch, C., Dybkjær, K., & Outridge, P. M. (2019). Volcanic mercury and mutagenesis in land plants during the end-Triassic mass extinction. *Science Advances*, 5(10). <https://doi.org/10.1126/sciadv.aaw4018>
- Liu, M., Zhang, Q., Maavara, T., Liu, S., Wang, X., & Raymond, P. A. (2021). Rivers as the largest source of mercury to coastal oceans worldwide. *Nature Geoscience*, 14(9), 672–677. <https://doi.org/10.1038/s41561-021-00793-2>
- Liu, Y., Li, Y., Hou, M., Shen, J., Algeo, T. J., Fan, J., Zhou, X., Chen, Q., Sun, Z., & Li, C. (2023). Terrestrial rather than volcanic mercury inputs to the Yangtze Platform (South China) during the Ordovician-Silurian transition. *Global and Planetary Change*, 220, 104023. <https://doi.org/10.1016/j.gloplacha.2022.104023>
- Liu, Z., Percival, L. M. E., Vandeputte, D., Selby, D., Claes, P., Over, D. J., & Gao, Y. (2021). Upper Devonian mercury record from North America and its implications for the Frasnian-Famennian mass extinction. *Palaeogeography, Palaeoclimatology, Palaeoecology*, 576, 110502. <https://doi.org/10.1016/j.palaeo.2021.110502>
- Lyons, T. W., & Berner, R. A. (1992). Carbon-sulfur-iron systematics of the uppermost deep-water sediments of the Black Sea. *Chemical Geology*, 99(1–3), 1–27. [https://doi.org/10.1016/0009-2541\(92\)90028-4](https://doi.org/10.1016/0009-2541(92)90028-4)

- Lyons, T. W., & Severmann, S. (2006). A critical look at iron paleoredox proxies: New insights from modern euxinic marine basins. *Geochimica et Cosmochimica Acta*, 70(23), 5698–5722. <https://doi.org/10.1016/j.gca.2006.08.021>
- Mason, R. P., Kim, E.-H., Cornwell, J., & Heyes, D. (2006). An examination of the factors influencing the flux of mercury, methylmercury and other constituents from estuarine sediment. *Marine Chemistry*, 102(1–2), 96–110. <https://doi.org/10.1016/j.marchem.2005.09.021>
- Moore, C. R., Brooks, M. J., Goodyear, A. C., Ferguson, T. A., Perrotti, A. G., Mitra, S., Listeck, A. M., King, B. C., Mallinson, D. J., Lane, C. S., Kapp, J. D., West, A., Carlson, D. L., Wolbach, W. S., Them, T. R., II, Harris, M. S., & Pyne-O'Donnell, S. (2019). Sediment Cores from White Pond, South Carolina, contain a Platinum Anomaly, Pyrogenic Carbon Peak, and Coprophilous Spore Decline at 12.8 ka. *Scientific Reports*, 9(1). <https://doi.org/10.1038/s41598-019-51552-8>
- Obrist, D., Moosmüller, H., Schürmann, R., Chen, L.-W. A., & Kreidenweis, S. M. (2008). Particulate-phase and gaseous elemental mercury emissions during biomass combustion: Controlling factors and correlation with particulate matter emissions. *Environmental Science & Technology*, 42(3), 721–727. <https://doi.org/10.1021/es071279n>
- Ostrander, C. M., Owens, J. D., & Nielsen, S. G. (2017). Constraining the rate of oceanic deoxygenation leading up to a Cretaceous Oceanic Anoxic Event (OAE-2: ~94 Ma). *Science Advances*, 3(8). <https://doi.org/10.1126/sciadv.1701020>
- Owens, J. D., Lyons, T. W., & Lowery, C. M. (2018). Quantifying the missing sink for global organic carbon burial during a Cretaceous oceanic anoxic event. *Earth and Planetary Science Letters*, 499, 83–94. <https://doi.org/10.1016/j.epsl.2018.07.021>
- Owens, J. D., Reinhard, C. T., Rohrssen, M., Love, G. D., & Lyons, T. W. (2016). Empirical links between trace metal cycling and marine microbial ecology during a large perturbation to Earth's carbon cycle. *Earth and Planetary Science Letters*, 449, 407–417. <https://doi.org/10.1016/j.epsl.2016.05.046>
- Pagani, M., Arthur, M. A., & Freeman, K. H. (1999). Miocene evolution of atmospheric carbon dioxide. *Paleoceanography*, 14(3), 273–292. <https://doi.org/10.1029/1999pa900006>
- Park, J., Stein, H. J., Georgiev, S. V., & Hannah, J. L. (2022). Degradation of Hg signals on incipient weathering: Core versus outcrop geochemistry of Upper Permian shales, East Greenland and Mid-Norwegian Shelf. *Chemical Geology*, 608, 121030. <https://doi.org/10.1016/j.chemgeo.2022.121030>
- Percival, L. M. E., Bergquist, B. A., Mather, T. A., & Sanei, H. (2021). Sedimentary Mercury Enrichments as a Tracer of Large Igneous Province Volcanism. In *Geophysical Monograph Series* (pp. 247–262). <https://doi.org/10.1002/9781119507444.ch11>
- Percival, L. M. E., Jenkyns, H. C., Mather, T. A., Dickson, A. J., Batenburg, S. J., Ruhl, M., Hesselbo, S. P., Barclay, R., Jarvis, I., Robinson, S. A., & Woelders, L. (2018). Does large igneous province volcanism always perturb the mercury cycle? Comparing the records of Oceanic Anoxic Event 2 and the end-Cretaceous to other Mesozoic events. *American Journal of Science*, 318(8), 799–860. <https://doi.org/10.2475/08.2018.01>
- Petsch, S. T., Berner, R. A., & Eglinton, T. I. (2000). A field study of the chemical weathering of ancient sedimentary organic matter. *Organic Geochemistry*, 31(5), 475–487. [https://doi.org/10.1016/S0146-6380\(00\)00014-0](https://doi.org/10.1016/S0146-6380(00)00014-0)
- Pippenger, K. H., Estrada, L., Jones, D. S., & Cohen, P. A. (2023). Appalachian Basin mercury enrichments during the Late Devonian Kellwasser Events and comparison to global records. *Palaeogeography, Palaeoclimatology, Palaeoecology*, 627, 111751. <https://doi.org/10.1016/j.palaeo.2023.111751>
- Pirrone, N., Cinnirella, S., Feng, X., Finkelman, R. B., Friedli, H. R., Leaner, J., Mason, R., Mukherjee, A. B., Stracher, G. B., Streets, D. G., & Telmer, K. (2010). Global mercury emissions to the atmosphere from anthropogenic and natural sources. *Atmospheric Chemistry and Physics*, 10(13), 5951–5964. <https://doi.org/10.5194/acp-10-5951-2010>
- Pisciotta, K. A., & Garrison, R. E. (1981). Lithofacies and Depositional Environments of the Monterey Formation, California. In R. E. Garrison & R. G. Douglas (Eds.), *The Monterey Formation and related siliceous rocks of California: Los Angeles* (pp. 97–122). Pacific Section, SEPM.
- Pruss, S. B., Jones, D. S., Fike, D. A., Tosca, N. J., & Wignall, P. B. (2019). Marine anoxia and sedimentary mercury enrichments during the Late Cambrian SPICE event in northern Scotland. *Geology*, 47(5), 475–478. <https://doi.org/10.1130/g45871.1>
- Pyle, D. M., & Mather, T. A. (2003). The importance of volcanic emissions for the global atmospheric mercury cycle. *Atmospheric Environment*, 37(36), 5115–5124. <https://doi.org/10.1016/j.atmosenv.2003.07.011>
- Pytte, M. H. (1989). Comparison of Monterey formation kerogens from the Salinas Basin and Santa Barbara area, California. *Organic Geochemistry*, 14(3), 233–245. [https://doi.org/10.1016/0146-6380\(89\)90052-1](https://doi.org/10.1016/0146-6380(89)90052-1)

- Rahman, H. M., Kennedy, M., Löhr, S., & Dewhurst, D. N. (2017). Clay-organic association as a control on hydrocarbon generation in shale. *Organic Geochemistry*, *105*, 42–55. <https://doi.org/10.1016/j.orggeochem.2017.01.011>
- Rakociński, M., Marynowski, L., Piszczowska, A., Bełdowski, J., Siedlewicz, G., Zatoń, M., Perri, M. C., Spalletta, C., & Schönlaub, H. P. (2020). Volcanic related methylmercury poisoning as the possible driver of the end-Devonian Mass Extinction. *Scientific Reports*, *10*(1). <https://doi.org/10.1038/s41598-020-64104-2>
- Raven, M. R., Adkins, J. F., Werne, J. P., Lyons, T. W., & Sessions, A. L. (2015). Sulfur isotopic composition of individual organic compounds from Cariaco Basin sediments. *Organic Geochemistry*, *80*, 53–59. <https://doi.org/10.1016/j.orggeochem.2015.01.002>
- Raven, M. R., Fike, D. A., Gomes, M. L., Webb, S. M., Bradley, A. S., & McClelland, H.-L. O. (2018). Organic carbon burial during OAE2 driven by changes in the locus of organic matter sulfurization. *Nature Communications*, *9*(1). <https://doi.org/10.1038/s41467-018-05943-6>
- Ravichandran, M. (2004). Interactions between mercury and dissolved organic matter--a review. *Chemosphere*, *55*(3), 319–331. <https://doi.org/10.1016/j.chemosphere.2003.11.011>
- Retallack, G. J. (2001). Cenozoic expansion of grasslands and climatic cooling. *The Journal of Geology*, *109*(4), 407–426. <https://doi.org/10.1086/320791>
- Ruhl, M., Hesselbo, S. P., Al-Suwaidi, A., Jenkyns, H. C., Damborenea, S. E., Manceñido, M. O., Storm, M., Mather, T. A., & Riccardi, A. C. (2020). On the onset of Central Atlantic Magmatic Province (CAMP) volcanism and environmental and carbon-cycle change at the Triassic-Jurassic transition (Neuquén Basin, Argentina). *Earth-Science Reviews*, *208*, 103229. <https://doi.org/10.1016/j.earscirev.2020.103229>
- Schuster, P. F., Schaefer, K. M., Aiken, G. R., Antweiler, R. C., Dewild, J. F., Gryziec, J. D., Gusmeroli, A., Hugelius, G., Jafarov, E., Krabbenhoft, D. P., Liu, L., Herman-Mercer, N., Mu, C., Roth, D. A., Schaefer, T., Striegl, R. G., Wickland, K. P., & Zhang, T. (2018). Permafrost Stores a Globally Significant Amount of Mercury. *Geophysical Research Letters*, *45*(3), 1463–1471. <https://doi.org/10.1002/2017gl075571>
- Scott, C., & Lyons, T. W. (2012). Contrasting molybdenum cycling and isotopic properties in euxinic versus non-euxinic sediments and sedimentary rocks: Refining the paleoproxies. *Chemical Geology*, *324–325*, 19–27. <https://doi.org/10.1016/j.chemgeo.2012.05.012>
- Scott, C., Lyons, T. W., Bekker, A., Shen, Y., Poulton, S. W., Chu, X., & Anbar, A. D. (2008). Tracing the stepwise oxygenation of the Proterozoic ocean. *Nature*, *452*(7186), 456–459. <https://doi.org/10.1038/nature06811>
- Selin, N. E. (2009). Global Biogeochemical Cycling of Mercury: A Review. *Annual Review of Environment and Resources*, *34*(1), 43–63. <https://doi.org/10.1146/annurev.environ.051308.084314>
- Severmann, S., Lyons, T. W., Anbar, A., McManus, J., & Gordon, G. (2008). Modern iron isotope perspective on the benthic iron shuttle and the redox evolution of ancient oceans. *Geology*, *36*(6), 487. <https://doi.org/10.1130/g24670a.1>
- Shen, J., Algeo, T. J., Chen, J., Planavsky, N. J., Feng, Q., Yu, J., & Liu, J. (2019). Mercury in marine Ordovician/Silurian boundary sections of South China is sulfide-hosted and non-volcanic in origin. *Earth and Planetary Science Letters*, *511*, 130–140. <https://doi.org/10.1016/j.epsl.2019.01.028>
- Shen, J., Feng, Q., Algeo, T. J., Liu, J., Zhou, C., Wei, W., Liu, J., Them, T. R., II, Gill, B. C., & Chen, J. (2020). Sedimentary host phases of mercury (Hg) and implications for use of Hg as a volcanic proxy. *Earth and Planetary Science Letters*, *543*, 116333. <https://doi.org/10.1016/j.epsl.2020.116333>
- Sosdian, S. M., Babila, T. L., Greenop, R., Foster, G. L., & Lear, C. H. (2020). Ocean Carbon Storage across the middle Miocene: a new interpretation for the Monterey Event. *Nature Communications*, *11*(1). <https://doi.org/10.1038/s41467-019-13792-0>
- Stanley, R. G., Wilson, D. S., & McCrory, P. A. (2000). *Locations and ages of middle Tertiary volcanic centers in coastal California*. U.S. Geological Survey. <https://doi.org/10.3133/ofr00154>
- Steinthorsdottir, M., Jardine, P. E., & Rember, W. C. (2021). Near-Future pCO<sub>2</sub> During the Hot Miocene Climatic Optimum. *Paleoceanography and Paleoclimatology*, *36*(1). <https://doi.org/10.1029/2020pa003900>
- Strömberg, C. A. E. (2011). Evolution of Grasses and Grassland Ecosystems. *Annual Review of Earth and Planetary Sciences*, *39*(1), 517–544. <https://doi.org/10.1146/annurev-earth-040809-152402>
- Sun, R., Jiskra, M., Amos, H. M., Zhang, Y., Sunderland, E. M., & Sonke, J. E. (2019). Modelling the mercury stable isotope distribution of Earth surface reservoirs: Implications for global Hg cycling. *Geochimica et Cosmochimica Acta*, *246*, 156–173. <https://doi.org/10.1016/j.gca.2018.11.036>

- Them, T. R., II, Gill, B. C., Caruthers, A. H., Gröcke, D. R., Tulsy, E. T., Martindale, R. C., Poulton, T. P., & Smith, P. L. (2017). High-resolution carbon isotope records of the Toarcian Oceanic Anoxic Event (Early Jurassic) from North America and implications for the global drivers of the Toarcian carbon cycle. *Earth and Planetary Science Letters*, 459, 118–126. <https://doi.org/10.1016/j.epsl.2016.11.021>
- Them, T. R., II, Jagoe, C. H., Caruthers, A. H., Gill, B. C., Grasby, S. E., Gröcke, D. R., Yin, R., & Owens, J. D. (2019). Terrestrial sources as the primary delivery mechanism of mercury to the oceans across the Toarcian Oceanic Anoxic Event (Early Jurassic). *Earth and Planetary Science Letters*, 507, 62–72. <https://doi.org/10.1016/j.epsl.2018.11.029>
- Them, T. R., II, Owens, J. D., Marroquín, S. M., Caruthers, A. H., Alexandre, J. P. T., & Gill, B. C. (2022). Reduced Marine Molybdenum Inventory Related to Enhanced Organic Carbon Burial and an Expansion of Reducing Environments in the Toarcian (Early Jurassic) Oceans. *AGU Advances*, 3(6). <https://doi.org/10.1029/2022av000671>
- Tisserand, D., Guédron, S., Viollier, E., Jézéquel, D., Rigaud, S., Campillo, S., Sarret, G., Charlet, L., & Cossa, D. (2022). Mercury, organic matter, iron, and sulfur co-cycling in a ferruginous meromictic lake. *Applied Geochemistry*, 146, 105463. <https://doi.org/10.1016/j.apgeochem.2022.105463>
- Tremblin, M., Khozyem, H., Adatte, T., Spangenberg, J. E., Fillon, C., Grauls, A., Hunger, T., Nowak, A., Läuchli, C., Lasseur, E., Roig, J.-Y., Serrano, O., Calassou, S., Guillocheau, F., & Castelltort, S. (2022). Mercury enrichments of the Pyrenean foreland basins sediments support enhanced volcanism during the Paleocene-Eocene thermal maximum (PETM). *Global and Planetary Change*, 212, 103794. <https://doi.org/10.1016/j.gloplacha.2022.103794>
- Tribouillard, N., Algeo, T. J., Lyons, T., & Riboulleau, A. (2006). Trace metals as paleoredox and paleoproductivity proxies: An update. *Chemical Geology*, 232(1–2), 12–32. <https://doi.org/10.1016/j.chemgeo.2006.02.012>
- Tuttle, M. L. W., & Breit, G. N. (2009). Weathering of the New Albany Shale, Kentucky, USA: I. Weathering zones defined by mineralogy and major-element composition. *Applied Geochemistry*, 24(8), 1549–1564. <https://doi.org/10.1016/j.apgeochem.2009.04.021>
- von der Heydt, A., & Dijkstra, H. A. (2008). The effect of gateways on ocean circulation patterns in the Cenozoic. *Global and Planetary Change*, 62(1–2), 132–146. <https://doi.org/10.1016/j.gloplacha.2007.11.006>
- Weigand, P. W., Savage, K. L., & Nicholson, C. (2002). The Conejo Volcanics and other Miocene volcanic suites in southwestern California. In *Contributions to Crustal Evolution of the Southwestern United States*. <https://doi.org/10.1130/0-8137-2365-5.187>
- Werne, J. P., Lyons, T. W., Hollander, D. J., Formolo, M. J., & Sinningh Damsté, J. S. (2003). Reduced sulfur in euxinic sediments of the Cariaco Basin: sulfur isotope constraints on organic sulfur formation. *Chemical Geology*, 195(1–4), 159–179. [https://doi.org/10.1016/s0009-2541\(02\)00393-5](https://doi.org/10.1016/s0009-2541(02)00393-5)
- Westerhold, T., Bickert, T., & Röhl, U. (2005). Middle to late Miocene oxygen isotope stratigraphy of ODP site 1085 (SE Atlantic): new constraints on Miocene climate variability and sea-level fluctuations. *Palaeogeography, Palaeoclimatology, Palaeoecology*, 217(3–4), 205–222. <https://doi.org/10.1016/j.palaeo.2004.12.001>
- White, L. D., Garrison, R. E., & Barron, J. A. (1992). Miocene intensification of upwelling along the California margin as recorded in siliceous facies of the Monterey Formation and offshore DSDP sites. *Geological Society, London, Special Publications*, 64(1), 429–442. <https://doi.org/10.1144/gsl.sp.1992.064.01.28>
- Wildman, R. A., Berner, R. A., Petsch, S. T., Bolton, E. W., Eckert, J. O., Mok, U., & Evans, J. B. (2004). The weathering of sedimentary organic matter as a control on atmospheric O<sub>2</sub>: I. Analysis of a black shale. *American Journal of Science*, 304(3), 234–249. <https://doi.org/10.2475/ajs.304.3.234>
- Woodring, W. P., & Bramlette, M. N. (1950). *Geology and paleontology of the Santa Maria district, California*. Professional Paper. <https://doi.org/10.3133/pp222>
- Woodruff, F., & Savin, S. M. (1989). Miocene deepwater oceanography. *Paleoceanography*, 4(1), 87–140. <https://doi.org/10.1029/pa004i001p00087>
- Wright, J. D., Miller, K. G., & Fairbanks, R. G. (1992). Early and Middle Miocene stable isotopes: Implications for Deepwater circulation and climate. *Paleoceanography*, 7(3), 357–389. <https://doi.org/10.1029/92pa00760>
- Zachos, J., Pagani, M., Sloan, L., Thomas, E., & Billups, K. (2001). Trends, rhythms, and aberrations in global climate 65 Ma to present. *Science*, 292(5517), 686–693. <https://doi.org/10.1126/science.1059412>
- Zaferani, S., Pérez-Rodríguez, M., & Biester, H. (2018). Diatom ooze—A large marine mercury sink. *Science*, 361(6404), 797–800. <https://doi.org/10.1126/science.aat2735>



Zhu, W., Song, Y., Adediran, G. A., Jiang, T., Reis, A. T., Pereira, E., Skjellberg, U., & Björn, E. (2018). Mercury transformations in resuspended contaminated sediment controlled by redox conditions, chemical speciation and sources of organic matter. *Geochimica et Cosmochimica Acta*, 220, 158–179. <https://doi.org/10.1016/j.gca.2017.09.045>

## SUPPLEMENTARY MATERIALS

### **Geochemical data from Miocene Monterey Formation**

Download: <https://ajsonline.org/article/122687-organic-rich-shales-reveal-local-controls-that-enhanced-mercury-accumulation-during-a-non-lip-interval-of-the-miocene-implications-for-the-mercury-pa/attachment/247319.xlsx>

---